IVYSPRING INTERNATIONAL PUBLISHER

Theranostics

2024; 14(10): 4127-4146. doi: 10.7150/thno.97768

Review

Biomarker-driven molecular imaging probes in radiotherapy

Haonan Li[1], Qiyong Gong[1,2,3,✉], Kui Luo[1,2,✉]

1. Department of Radiology, Huaxi MR Research Center (HMRRC), Frontiers Science Center for Disease-Related Molecular Network, State Key Laboratory of Biotherapy, West China Hospital, Sichuan University, No. 37 Guoxue Alley, Chengdu 610041, China.
2. Functional and Molecular Imaging Key Laboratory of Sichuan Province and Research Unit of Psychoradiology, Chinese Academy of Medical Sciences, Chengdu 610041, China.
3. Department of Radiology, West China Xiamen Hospital of Sichuan University, 699 Jinyuan Xi Road, Jimei District, 361021 Xiamen, Fujian, China.

✉ Corresponding authors: Prof. Qiyong Gong, E-mail: qiyonggong@hmrrc.org.cn. Prof. Kui Luo, E-mail: luokui@scu.edu.cn. **ORCID ID:** Haonan Li (https://orcid.org/0000-0002-0188-646X), Qiyong Gong (https://orcid.org/0000-0002-5912-4871), Kui Luo (https://orcid.org/0000-0002-3536-1485).

Received: 2024.04.25; Accepted: 2024.06.23; Published: 2024.07.02

Abstract

Background: Biomarker-driven molecular imaging has emerged as an integral part of cancer precision radiotherapy. The use of molecular imaging probes, including nanoprobes, have been explored in radiotherapy imaging to precisely and noninvasively monitor spatiotemporal distribution of biomarkers, potentially revealing tumor-killing mechanisms and therapy-induced adverse effects during radiation treatment.

Methods: We summarized literature reports from preclinical studies and clinical trials, which cover two main parts: 1) Clinically-investigated and emerging imaging biomarkers associated with radiotherapy, and 2) instrumental roles, functions, and activatable mechanisms of molecular imaging probes in the radiotherapy workflow. In addition, reflection and future perspectives are proposed.

Results: Numerous imaging biomarkers have been continuously explored in decades, while few of them have been successfully validated for their correlation with radiotherapeutic outcomes and/or radiation-induced toxicities. Meanwhile, activatable molecular imaging probes towards the emerging biomarkers have exhibited to be promising in animal or small-scale human studies for precision radiotherapy.

Conclusion: Biomarker-driven molecular imaging probes are essential for precision radiotherapy. Despite very inspiring preliminary results, validation of imaging biomarkers and rational design strategies of probes await robust and extensive investigations. Especially, the correlation between imaging biomarkers and radiotherapeutic outcomes/toxicities should be established through multi-center collaboration involving a large cohort of patients.

Keywords: biomarker, molecular imaging, radiotherapy, imaging probe, nanoparticle

1. Introduction

Radiotherapy prevails in routine clinical practice and plays a cornerstone role in anti-cancer therapy. Imaging, an indispensable part of radiotherapy, aids in delineation of the targeted tumor sub-volume for accurate determination of a uniform therapeutic dose or non-homogeneous dose distribution in the target area. Moreover, advanced clinical imaging tools, such as magnetic resonance imaging (MRI) or positron emission tomography (PET), have been integrated into a radiation system to provide detailed information on anatomy and response of patients before and during radiotherapy [1, 2]. Meanwhile, multiparametric MRI (mpMRI), various tracer-based nuclear medicine imaging techniques, and other imaging modalities have been implemented for post-radiotherapy assessment. However, current clinical imaging guidelines [3, 4], such as Response Evaluation Criteria in Solid tumours (RECIST), and RECIST for intratumoral therapies (itRECIST) and immunotherapy (iRECIST), fail to meet the requirements of therapy-specific and timely evaluation of routine and/or emerged combinational radiotherapies (i.e., radio-immunotherapy) [5, 6], whose response patterns may vary from previously

well-established one. In this context, novel advanced imaging tools in three main steps in combinational radiotherapies, namely radiotherapy planning, patient stratification, and response/toxicity assessment, are in urgent need [7].

Biomarker-driven molecular imaging has been explored to address these pressing clinical needs. Till now, several radiotherapy-related biomarkers have been identified, including tumor-specific biomarkers for targeted radiotherapy and patient stratification (e.g., prostate-specific membrane antigen (PSMA) and hypoxia) [8, 9], radiotherapy-derived biomarkers for assessment/prediction of tumor response and normal tissue toxicities (e.g., reactive oxygen species (ROS) and caspase-3) [10, 11], and imaging features extracted from functional images (e.g., standard uptake value (SUV) and multiple MRI parameters) [12, 13]. The medical research or clinical value of some of these biomarkers has been partially validated or validated in many prospective or retrospective clinical investigations, whereas other specific biomarkers for improving clinical decision-making processes remain to be unveiled, validated, and established. Encouragingly, molecular imaging probes, particularly nanoprobes with a high level of modifiability and multiple imaging modalities [14-17], have been developed to monitor the tumor microenvironment before, during, and after radiation-based therapies in a manner of biomarker-driven activatable imaging. In this context, these imaging probes could be tuned for targeting well-established biomarkers with biological significance, thus offering dynamic and spatiotemporal information for personalized precision therapy to achieve great clinical benefits for cancer patients.

Herein, radiotherapy-specific or its derived imaging biomarkers are surveyed in Chapter 2. Molecular imaging probes for these biomarkers have been developed for imaging-guided/assisted radiotherapy (radiotherapy planning), patient stratification, response assessment, and toxicity/resistance prediction (Chapter 3). Reflection and future perspectives of this biomarker-based molecular imaging for precision radiotherapy are provided in Chapter 4.

2. Molecular imaging and imaging biomarkers for cancer radiotherapy

2.1. Molecular imaging in radiation oncology

Beyond providing anatomic information, molecular imaging aims to provide fundamental insights/understandings into the pathophysiological process at the molecular and cellular levels under various diseases or therapies-induced changes, thus helping with clinical decision-making. In the context of radiation oncology, molecular imaging with improved specificity and sensitivity plays an important role in radiotherapy planning (e.g., diagnosis and staging, target definition, and image-guided radiotherapy before dose delivery) and early/late-stage treatment response assessment.

In current clinical practice, PET/CT with improved spatial and contrast resolutions and multiparametric MRI are the main workforce, while in preclinical studies, optical imaging, particularly photoacoustic imaging and near-infrared imaging, has emerged. These advanced imaging modalities have been devoted to detecting the minor or significant changes of biomarkers associated with cancer or the radiotherapy-involved pathophysiological process, including but not limited to receptors, cell adhesion molecules, hypoxia, apoptosis, and angiogenesis.

2.2. Overview of imaging biomarkers

Broadly speaking, molecular, histologic, radiographic, or physiologic characteristics are examples of biomarkers [18]. The multifaceted types of biomarkers have different definitions and classifications [19]. In this review, we define their types in radiotherapy (external beam radiation therapy (EBRT), brachytherapy, and radiopharmaceutical therapy (RPT)), varying from diagnostics, prognostics, prediction, and toxicity assessment. To note, biomarkers associated with radiotherapy for indicating biological changes in molecules/proteins, intracellular organelles, cells, and tissues/organs, will be explored and discussed in this review [20]. Clinically-investigated biomarkers, such as radiological findings (diametric expansion rate) [21], early metabolic response [22], and imaging parameters [23], will also be briefly mentioned. Additionally, we will specifically discuss the biomarkers that could be employed to develop non-invasive imaging techniques and spatiotemporally assesses tumor lesions (one or more sites) *in vivo* in this review article. Biomarkers that are associated with radiotherapy but cannot be imaged [24], including transcriptomic biomarkers, human papillomavirus (HPV), gene profiles, and extracellular vesicles, are beyond the scope of this review.

2.3. Clinically-investigated and emerging imaging biomarkers

In routine clinical practices, PET and/or MR imaging of hypoxia and metabolic responses prevail in radiotherapy planning and treatment assessment, respectively [23, 25, 26]. Moreover, several promising imaging biomarkers and novel imaging techniques

have been emerged in pre-clinical studies (**Figure 1**).

Table 1. Representative clinically-used or investigated biomarkers for imaging hypoxia.

Biomarkers	Imaging methods	Refs
Hypoxic biological features	2-nitroimidazole compounds-based PET tracers (^{18}F-FMISO, ^{18}F-FETNIM, and ^{18}F-FAZA) or SPECT tracers	[28]
	^{64}Cu-ATSM PET tracer	[29]
	^{99m}Tc-labelled SPECT tracer	[30]
	^{123}I-IAZA SPECT tracer	[31]
pO_2	^{19}F-relaxometry	[32]
	EPRI oximetry	[33]
	Fiber-optic oxygen-sensing devices	[34]
Perfusion	Dynamic contrast enhanced MRI	[35]
	Computed tomography	[36]
Hemoglobin-oxygen saturation	*R2** (Spin dephasing rates) from MRI BOLD sequence	[37]
	Photoacoustic imaging	[38]

PET: positron emission tomography; FMISO: fluoromisonidazole; FETNIM: fluoroerythronitroimidazole; FAZA: fluoroazomycin arabinoside; SPECT: single photon emission computed tomography; Cu-ATSM: Copper (II)-diacetyl-bis(4-methyl-3-thiosemicarbazone); IAZA: iodoazomycin arabinoside; pO_2: intratumoral oxygen partial pressure; EPRI: electron paramagnetic resonance imaging; BOLD: blood-oxygen-level-dependent.

Hypoxia. Intratumoral oxygen partial pressure (pO_2) and hypoxia-induced pathophysiological changes (e.g., upregulated expression of nitroreductase) are typical biomarkers for imaging hypoxia [9]. Imaging methods for these biomarkers are summarized in **Table 1**. In clinical practices, validated hypoxia measurements have been realized through diagnostic targeted PET probes and MRI techniques, whereas emerged imaging techniques, such as MRI-chemical exchange saturation transfer (CEST) pH imaging and photoacoustic imaging have recently gained popularity for imaging and grading hypoxia [27].

Metabolic responses. Functional multiparametric magnetic resonance imaging (mpMRI) and 2-[^{18}F]fluoro-2-deoxy-D-glucose (^{18}F-FDG) PET/CT are two major methods to detect early metabolic responses after radiotherapy [39, 40]. These imaging results as early predictors, such as apparent diffusion coefficient (ADC), magnetic resonance spectroscopy (MRS), standardized uptake value (SUV) and total lesion glycolysis (TLG), have been frequently explored in radiotherapy for a variety of tumor indications (e.g., esophageal cancer, soft tissue sarcoma) [41, 42]. Furthermore, these imaging results in radiotherapy have been reported to be correlated with end points such as recurrence-free survival (RFS) or overall survival (OS) in several prospective/retrospective studies [43-45]. For instance, an increased value in the ADC was reported to has a

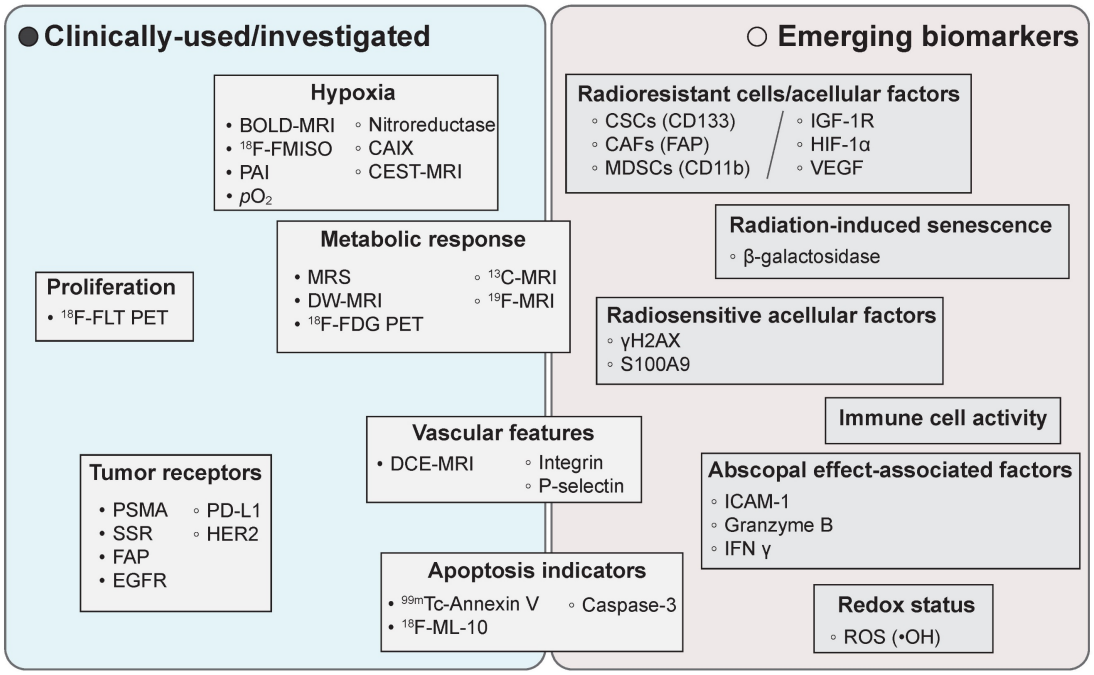

Figure 1. Representative clinically-used/investigated and emerging imaging biomarkers in radiation oncology. BOLD: blood oxygen level dependent; MRI: magnetic resonance imaging; FMISO: fluoromisonidazole; PAI: photoacoustic imaging; CAIX: carbonic anhydrase IX; CEST: chemical exchange saturation transfer; ^{18}F-FLT: 3'-deoxy-3'-([^{18}F]Fluoro)-fluorothymidine; PET: positron emission tomography; MRS: magnetic resonance spectroscopy; DW-MRI: diffusion-weighted MRI; ^{18}F-FDG: 2-[^{18}F]fluoro-2-deoxy-D-glucose; PSMA: prostate-specific membrane antigen; SSR: somatostatin receptor; FAP: fibroblast activation protein; EGFR: epidermal growth factor receptor; PD-L1: programmed death-ligand 1; HER2: human epidermal growth factor receptor 2; DCE: dynamic contrast-enhanced; CSCs: cancer stem cells; CAFs: cancer-associated fibroblasts; MDSCs: myeloid-derived suppressor cells; IGF-1R: insulin-like growth factor 1 receptor; VEGF: vascular endothelial growth factor; ICAM-1: intercellular cell adhesion molecule-1; IFNγ: interferon-γ; ROS: reactive oxygen species.

positive correlation with better local control and progression-free survival for mid-RT of head and neck cancer in one prospective study involving 81 patients with a median follow-up of 31 months [43], as well as a declined ADC value after radiotherapy was related with an increased chance of clinical recurrence in a multicenter retrospective analysis of 229 prostate cancer patients [44]. In a prospective study involving 62 patients with HPV-related oropharyngeal cancer, SUV, an early PET parameter after 2 weeks of definitive RT (~ 20 Gy), was found to be correlated with RFS and OS [45]. In addition, emerged imaging techniques, such as hyperpolarized ^{13}C MRI, have been reported to aid in accelerating early detection of metabolic responses (e.g., pyruvate metabolism) as early as 1 day after radiotherapy [46]. However, ^{18}F-FDG PET/CT lacks specificity, thus it is very challenging to differentiate glucose changes in the brain and liver due to inflammation or radiotherapy. In addition, the ^{18}F-FDG uptake rate is only slightly elevated in aggressive subtypes of prostate cancer and neuroendocrine tumors. Other clinically available nuclear imaging probes, e.g., [^{18}F]FIMP, have been explored for early-phase assessment of radiotherapeutic responses [47].

Tumor-associated surface receptors. The prostate specific membrane antigen (PSMA) highly expressed on prostate cancer cells and the majority of neovasculature of most solid tumors, and the somatostatin receptor (SSR) highly expressed on neuroendocrine tumors have been successful biomarkers in clinic practices for assisting in both EBRT and RPT in the terms of treatment planning and dosimetry guidance [8, 48]. For instance, ^{68}Ga-PSMA11 and ^{68}Ga-DOTATATE PET probes have been routinely used in the companion diagnosis to adjust the therapeutic dose of ^{177}Lu-PSMA617 and ^{177}Lu-DOTATATE for patients with prostate cancer or neuroendocrine tumors, respectively. Furthermore, in a recent report, an early change of total lesion PSMA (TLP) (p = 0.002) had been found to outperform the serum PSA-based response (p = 0.515) in predicting overall survival in 66 metastatic castration-resistant prostate cancer patients treated with ^{177}Lu-PSMA617 [48]. Some other receptors (e.g., fibroblast activation protein (FAP), epidermal growth-factor receptor (EGFR), and integrin $\alpha_v\beta_3$) with the similar function have also been experimented and trialed [49, 50].

Radioresistant cell types. The density of cancer stem cells (CSCs) (CD133) [51], CSCs-mediated repopulation with increased epidermal growth factor receptor (EGFR) expression [52], the postradiotherapy cancer stemness [53], cancer-associated fibroblast heterogeneity [49, 50], and myeloid-derived suppressor cells and neutrophils are risk factors for radioresistance [54]. Imaging probes, such as αCD133-CF770 and [^{89}Zr]Zr-DFO-αCD133 have been employed to image CSCs in small cell lung cancer (SCLC) [55]. In addition, ^{89}Zr-labeled PEGylated anti-CD11b VHHs (antigen binding fragment of heavy chain only antibodies) and [^{89}Zr]anti-CD11b antibody (clone M1/70) were reported for immune-PET imaging of the myeloid compartment in colorectal cancer or glioblastoma, respectively [56, 57].

Radioresistant acellular factors. Several biological factors have been identified to induce radioresistance, including DNA repair mechanisms (X-ray repair cross complementing family) [58], tyrosine kinases (insulin-like growth factor 1 receptor (IGF-1R)) [59], metabolic factors (hypoxia-inducible factor 1α, nuclear factor erythroid 2-related factor 2, cyclooxygenase-2), angiogenic regulators (vascular endothelial growth factor (VEGF), osteopontin, interleukin-6) [60], and other factors (NAPDH oxidase [61], galectin-1 [62], tissue factor (F3) [63]). For their corresponding imaging probes, ^{111}In-DOTA-$Z_{IGF1R:4551}$ was reported to image IGF-1R in DU-145 prostate cancer [64]; and bevacizumab was designed as a VEGF-A-targeting agent. Its derived imaging probes, including bevacizumab-800CW and gadolinium-diethylenetriaminepentaacetic acid-human serum albumin@indocyanine green-Bevacizumab, have been used in a phase 1 clinical trial to fluorescently visualize soft-tissue sarcomas [65], and guide breast cancer surgery and enhance radiotherapy, respectively [66].

Radiation therapy-induced senescence (TIS). TIS in tumor cells and T cells could be a contributing factor for radioresistance [67, 68]. β-galactosidase could be used to probe the senescent status in these cells [69]. For instance, a FL/PA bimodal probe, Gal-HCy-Biotin, and a NIR FL/MRI bimodal probe, Gal-Cy-Gd-1, have been reported for *in vivo* imaging of the β-galactosidase activity in tumors [67, 70]. In addition, radiation-induced endothelial senescence with a hallmark of the altered interleukin-1 signaling pathway has been found to be associated with lung tissue injury [71].

Radiosensitive factors. Protein biomarkers in human brain metastasis (e.g., S100A9) [72] and those involved in DNA damage response signaling pathways, such as residual γH2AX foci [73], can be used for in-vivo measurements of the intrinsic radiosensitivity level of tumor cells by employing corresponding imaging probes (for instance, [^{111}In]In-anti-γH2AX-TAT or [^{89}Zr]Zr-DFO-anti-γH2AX-TAT for measuring γH2AX foci).

Abscopal effect-associated factors. The abscopal effect, a phenomenon of the remission of nonirradiated or metastatic lesions beyond the

radiation field, occurs infrequently during radiotherapy and it can be attributed to radiotherapy-induced systematically antitumor immune response. Noninvasive imaging of intracellular adhesion molecule-1 (ICAM-1) and granzyme B, using a ^{89}Zr-DFO-αICAM-1/Fab PET probe and a DyLight 800- αICAM-1/Fab NIRF probe or a [^{68}Ga]-NOTA-GZP PET probe, respectively, has been employed for *in vivo* evaluation of the abscopal effect [74, 75]. Other upregulated factors, such as pro-inflammatory cytokine IFN γ, NKG2D ligand, and FAS receptor, may be potential imaging targets [76, 77]. However, the abscopal effect is not fully-understood yet and it often has poor reproducibility [78-81]. Recent reports have revealed that the blockade of the CD47/SIRPα axis would elicit a macrophage-mediated abscopal effect of radiotherapy and improve abscopal responses [82-84]. To note, the immunomodulatory effect may be indirectly assessed by the absolute lymphocyte counts [85] or the number of tumor-infiltrated immune effector cells.

Redox status. The radiotherapy efficacy is partially dependent on the redox potential in the tumor area, namely, the amount of generated hydroxyl radicals and other reactive oxygen species (ROS) after their interaction with antioxidants [86, 87]. Furthermore, concerns have been raised that antioxidants may promote cancer progression and metastasis [88], indirectly indicating the essential role of ROS in antitumor effects. In this context, the redox potential may be a promising predictive factor in response to conventional radiotherapy or radiosensitizers-enhanced radiotherapy [86]. For instance, *in vivo* dynamic nuclear polarization-MRI using a redox-sensitive carbamoyl-PROXYL probe has been explored for spatiotemporal evaluation of the redox status after radiotherapy [87].

Apoptosis indicators. Tumor apoptosis-associated markers, such as annexin V and caspase-3/7, also act as an initial indicator of radiotherapy efficacy. Based on these biological markers, a number of radiotracers, including ^{99m}Tc-Annexin V, ^{18}F-ML-10, ^{18}F-CP18, and ^{18}F-ICMT-11, have been developed to imaging apoptotic cells [89]. Moreover, in preclinical studies, caspase-3-responsive ratiometric photoacoustic imaging nanoprobes can be utilized for quantitative assessment of the applied radiation dose [90]. However, there is a debate on the role of caspase-3, and it has been argued that caspase may play a role in the cell death-induced tumor repopulation pathway during radiotherapy [91].

Tumor vascular-related indicators. Quantitative tumor-associated vasculature features, including vessel curvature, torsion, and organizational heterogeneity, have been exploited as an imaging biomarker for tumor response in multiple tumor types [92, 93] with the aid of imaging modalities, such as dynamic contrast-enhanced MRI. In addition, decreased tumor blood flow rates (e.g., more than 20%) and receptor expression (e.g., P-selectin) levels have been found to be positively correlated with therapeutic outcomes [94, 95].

3. Biomarker-driven molecular imaging probes in radiotherapy workflow

3.1. Strengths and roles of imaging probes in radiotherapy workflow

Imaging probes, comprised of small-molecules and nanoformulations, have unique strengths in their application in imaging [14-16, 96], including their inherent imaging properties, surface modifiability, and shape/size manipulability, thus, they have gained increasing interest in radiotherapy workflow. Strengths of applying state-of-the-art imaging probes before, during, and after radiotherapy are briefly listed below: a) Biomarker-specific single/dual/multiple-modality imaging. With the aid of elegant design of probes, such as biomarker-targeted or activated strategies and the use of bifunctional chelators, single/dual/multiple-modality imaging with great sensitivity/tumor penetration, sharp resolution, and enhanced signal-to-noise ratios could be realized [97-99]; b) Radiation-responsive imaging probes, such as a phenylalanine and tryptophan-based amino acid nanosensor gel and a gold-containing gel nanosensor [100-102], have been employed for radiation dosimetry in EBRT and/or RPT to quantitatively assess radiation exposure doses; c) X-ray-activated imaging probes, such as perovskite nanocrystal scintillators [103], organic phosphorescent scintillators [104], and probes with the properties of Cerenkov and radioluminescent light enhancement [105, 106], as well as organic luminophores with the ability of radio afterglow imaging [107], have been explored to supplement the contemporary cone beam CT-guided radiotherapy; and d) Probe-mediated immune cell-tracking for monitoring radiotherapy-induced immune response, including the distribution and activity of immune cells. Probe hitchhiking strategies or other direct/indirect cell labelling strategies aid in this tracking procedure [75, 108, 109].

Taken together, imaging probes, particularly nanoprobes, bring promising and substantial benefits in radiotherapy by broadening the imaging targets and achieving precision therapy through interaction with patient-specific biomarkers. Specific design of

them in the workflow of radiotherapy is illustrated in **Figure 2**. Mechanically, biomarker-responsive behaviors of imaging probes have been summarized in **Figure 3**.

3.2. Radiotherapy planning

In the current clinical setting, cone-beam computed tomography (CBCT)-guided linear accelerator radiation systems and two MRI-LINAC systems (0.35 T and 1.5 T) have been employed to radiotherapy planning and radiation delivery [110]. During biological image-guided adaptive radiotherapy, imaging biomarkers (e.g., markers for amino acids, phospholipid metabolism, peptides, cellular proliferation, hypoxia, and enzymatic activity) are essential to determine non-homogenous dose distribution in segmenting tumors for dose painting [111]. In this context, diagnostic biomarker-driven molecular imaging can accurately determine the gross tumor volume (GTV) and reduce the planning target volume (PTV) margin to improve tumor control probability or spare organs at risk (OARs) [112]. For instance, images obtained from biomarker-specific PET tracers, such as ^{68}Ga-DOTA-FAPI, ^{68}Ga-DOTATATE, and EGFR-targeted ^{89}Zr-Pantitumumab, could be useful for offline delineation of the GTV (e.g., intracranial meningiomas) [113, 114]. It has been revealed from a few clinical trials that greater clinical benefits, for instance, improvements in the failure-free survival [115], the median survival time [116], and the treatment tolerance [117], have been obtained by biological imaging-guided radiotherapy compared to the conventional imaging-guided one [118].

Accurate detection and delineation of GTV play a critical role in the determination of dose escalation or boosting. Tumor-specific biomarkers are often employed as imaging targets in this case, while these imaging biomarkers have to be carefully compared and verified. For instance, a fibroblast activation protein (FAP)-targeted ligand and a prostate-specific membrane antigen (PSMA)-targeted ligand were attached to the surface of core maghemite nanoparticles, respectively, and these nanoprobes were applied in MRI of orthotopic LNCaP prostate tumors. An about 15% improvement in the tumor contrast enhancement and a 1.5-fold increase in the R_2 values of the tumor periphery were seen in the group treated with FAP-targeted nanoprobes in comparison with the group with PSMA-targeted nanoprobes [119].

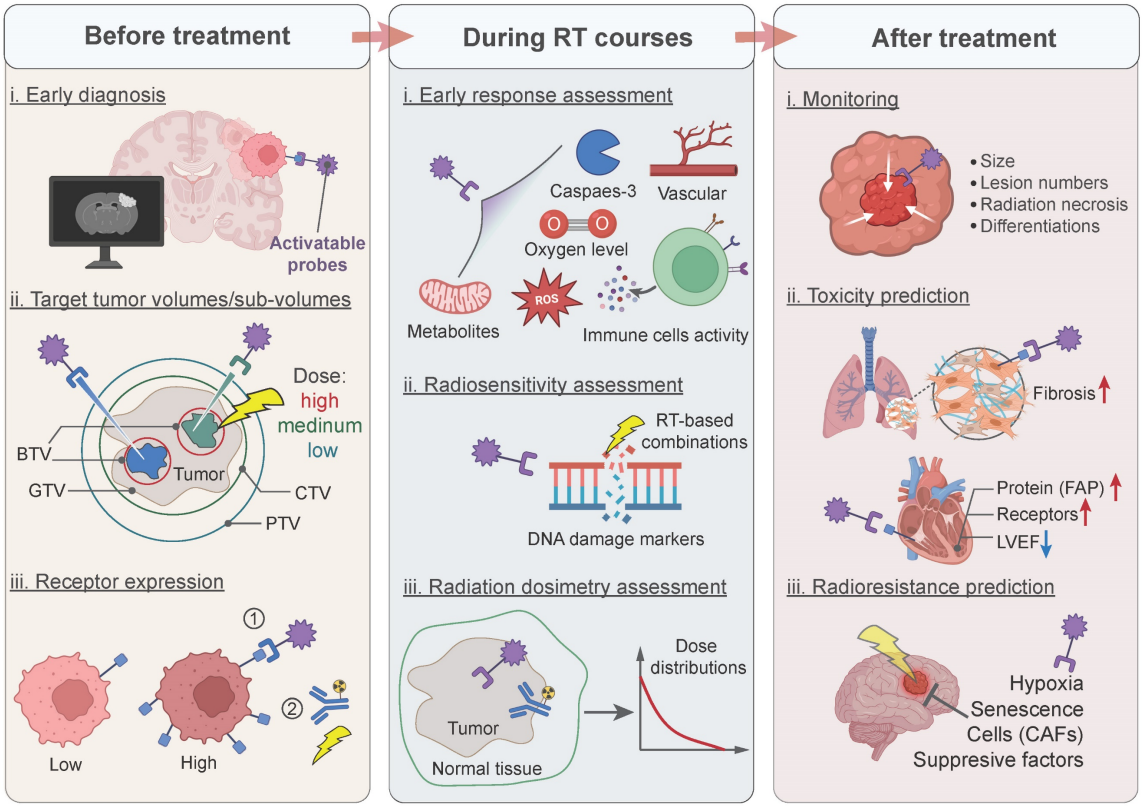

Figure 2. Application of activatable imaging probes in radiotherapy workflow. Before treatment: (i) diagnosing early-stage lesions; (ii) imaging different tumor sub-volumes for dose-escalation; (iii) monitoring the receptor expression for the selection of treatment methods. During radiotherapy courses: (i) assessing early tumor response; (ii) measuring the radiosensitivity index of radiotherapy; (iii) determining radiation dosimetry for optimizing treatment regimes. After treatment: (i) monitoring tumor progression and differentiating imaging results; (ii) predicting radiotherapy-induced toxicity for early interventions; (iii) predicting radioresistance for re-scheduling or changing treatment methods. BTV: biological target volume; GTV: gross tumor target volume; CTV: clinical target volume; PTV: planning target volume; FAP: fibroblast activation protein; LVEF: left ventricular ejection fraction; CAFs: cancer-associated fibroblasts.

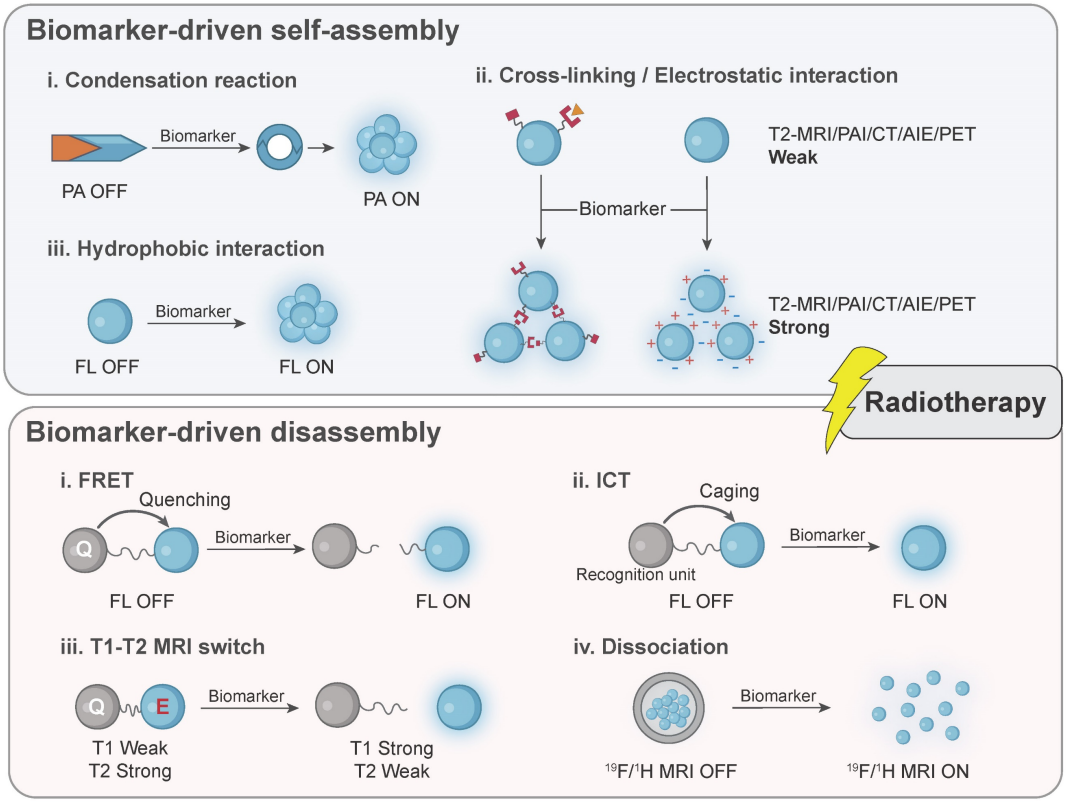

Figure 3. Activatable mechanisms of biomarker-driven imaging probes are divided into two major types: biomarker-driven self-assembly and biomarker-driven disassembly. In situ modification of probes is not illustrated in this scheme. PAI: photoacoustic imaging; MRI: magnetic resonance imaging; CT: computed tomography; AIE: aggregation-induced emission; PET: positron emission tomography; FL: fluorescence; FRET: fluorescence resonance energy transfer; ICT: intramolecular charge transfer.

Continuous efforts have been devoted to visualizing the hypoxic tumor sub-volume in modern precision radiotherapy planning, and the design strategy for probes is predominantly based on hypoxia-driven aggregation. A caspase-3 and GSH dual-responsive nanoprobe, consisting of a gold nanoparticle core and a coating containing a DEVD peptide-conjugated AIE molecule INT20, was constructed to realize an optical imaging-guided radiotherapy. The imaging enhancement was achieved through hypoxia-triggered aggregation of INT20 [120]. In one study, nitroimidazole derivatives as a hypoxia-sensitive ligand and cysteine in a certain ratio were conjugated to the surface of ultrasmall iron oxide nanoparticles, and an aggregation-responsive fluorescence dye, 4-chloro-7-nitro-2,1,3-benzoxadiazole (NBD), was incorporated into these nanoparticles. This dual-mode probe self-assembled via an intermolecular cross-linking mechanism in a hypoxia condition. Strong green fluorescence emitted from responsive NBD in this probe was seen in the 4T1 tumor tissue slices obtained from a hypoxic region-containing tumor with a volume of 1,000 cm^3 which was predominantly overlapped with a hypoxia marker, HIF-1α. This hypoxia-responsive probe also exhibited a 3.69-fold imaging signal enhancement in T2-weighted MRI (**Figure 4A**) [121]. In another study, surface coating of hypoxia-sensitive 2-(2-nitro-1*H*-imidazol-1-yl)ethanamine (NIE) and thiol compounds was applied to gold nanogaps. TEM images clearly indicated distinctive aggregation of nanoparticles when the incubation oxygen level dropped from 21% or 10%, to 1%. In addition, a 4.5-fold increase in the photoacoustic intensity in the in-vivo tumor area was credited to hypoxia-induced aggregation of probes, interestingly, an improvement in the radiotherapeutic efficacy by these gold nanoparticles suggested that they could be radiosensitizers [122].

Determination and utilization of the radiotherapy time window, such as the biological window of FLASH radiotherapy (a dose rate > 40 Gy/s), are essential for improving the therapy efficacy [123]. A pH and oxygen dual-sensitive $^{19}F/^{1}H$ CEST nanoprobe, Gly-PFOBs (glycerol-weighted and perfluorooctylbromide-based), was developed for imaging-guided lung cancer radiotherapy (**Figure 4B**). The period from 1 h 30 min to 2 h 30 min with a distinct feature of an increased pH was determined to be the optimized radiotherapy time window in an H209 SCLC liver metastasis model [32]. In addition, accurate assessment of the time to reach a peak for tumor accumulation of metal theranostic radiosensitizers (e.g., HfO_2, AGuIX, and iron oxide NPs) using corresponding imaging techniques is

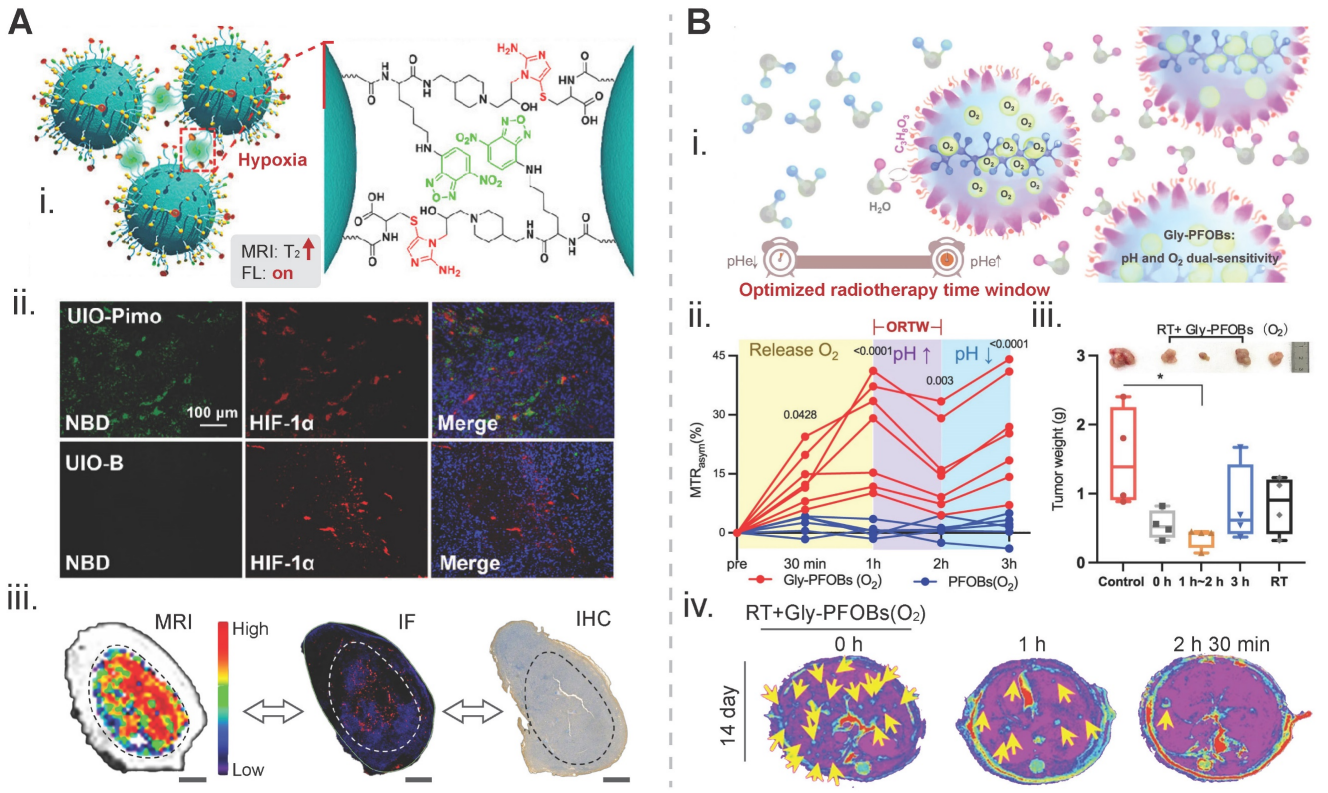

Figure 4. Biomarker-driven imaging probes for radiotherapy planning. A) Hypoxia-triggered self-assembly of an iron-oxide-based MRI/FL dual-mode nanoprobe, termed as UIO-Pimo, for delineation of the targeted tumor area: (i) design principles for imaging signal amplification; (ii) fluorescent images of tumor tissue slices. Red signal from HIF-1α indicates the hypoxia degree and the green signal from NBD represents the fluorescence of the activatable UIO-Pimo nanoprobe and a non-activatable UIO-B nanoprobe; (iii) the distribution of hypoxic areas within a tumor displayed via the nanoprobe-participated MRI difference value method. IF from HIF-1α, and IHC from commercial hypoxia indicator pimonidazole. Adapted with permission [121]. Copyright 2021 American Chemical Society. B) A pH/oxygen-activatable $^{19}F/^{1}H$ dual-mode nanoprobe for determining an optimal radiotherapeutic window: (i) scheme for the design of the nanoprobe; (ii) dynamic CEST signal changes in a NCI-H460 lung tumor area after injection of Gly-PFOB(O_2) or PFOB(O_2); (iii) tumor weights of each group on day 14 post-treatment. The time on the x axis indicats the duration of radiation treatment after injection of Gly-PFOB (O_2); (iv) T2WI MRI images of the liver in each treatment group, i.e., Gly-PFOB(O_2) + RT, Gly-PFOB(O_2) + RT at 1 h post injection of nanoprobe, and Gly-PFOB(O_2) + RT at 2 h 30 min post injection on day 14 post-treatment. Yellow arrows indicate liver metastasis. Adapted with permission [32]. Copyright 2023. Springer Nature. CC BY 4.0 (https://creativecommons.org/licenses/by/4.0/). MRI: magnetic resonance imaging; FL: fluorescence; HIF-1α: hypoxia-inducible factor-1 alpha; IF: immunofluorescence; IHC: immunohistochemistry.

critical for amplifying local radiation dose distribution and strengthening tumor cell damage after radiotherapy [124-126].

Overall, biomarkers-targeted imaging probes with high accuracy and specificity can be used to facilitate delineation of the biological-active tumor area, determine an optimal treatment window, and visualize the entire tumor tissue and affected lymph nodes, which will contribute to optimized radiotherapy planning [127]. Other radiotherapy guidance techniques using optical imaging are still in the proof-of-concept stage, and more efforts into the development of these techniques are required before they can be translated into clinical use.

3.3. Patient stratification

Biomarkers for early risk/benefit susceptibility/stratification could be imaged to distinguish patients with high-response from those with medium- or low-response and determine a patient cohort who is suitable for active surveillance or early intervention [128]. In radiopharmaceutical therapies, baseline PET or SPECT scans using biomarker-specific probes provide essential information for selecting patients who are eligible for peptide receptor radionuclide therapy [129, 130]. In external beam radiotherapy, molecular imaging of experimentally validated predictive biomarkers or biological features aids in selecting patients who will benefit from specific therapeutic methods. For instance, a multicenter retrospective study using PSMA-PET/CT has indicated that a high mean CT intensity in tumors with a cut-off of 19.7 HU was positively correlated with biochemical recurrence-free survival for patients receiving prostate salvage radiotherapy [131]. Overall, the patient stratification strategy helps screening a certain population of cancer patients to receive a beneficial therapy and avoid improper treatment or overtreatment. Oxygen levels, ROS levels, and caspase-3 have constituted typical biomarkers for early tumor stratification in radiotherapy [132-134]. Other biomarkers for radiotherapy stratification include the vascular density, metabolites, the intercellular cell adhesion molecule-1 (ICAM-1) (**Figure 5A**).

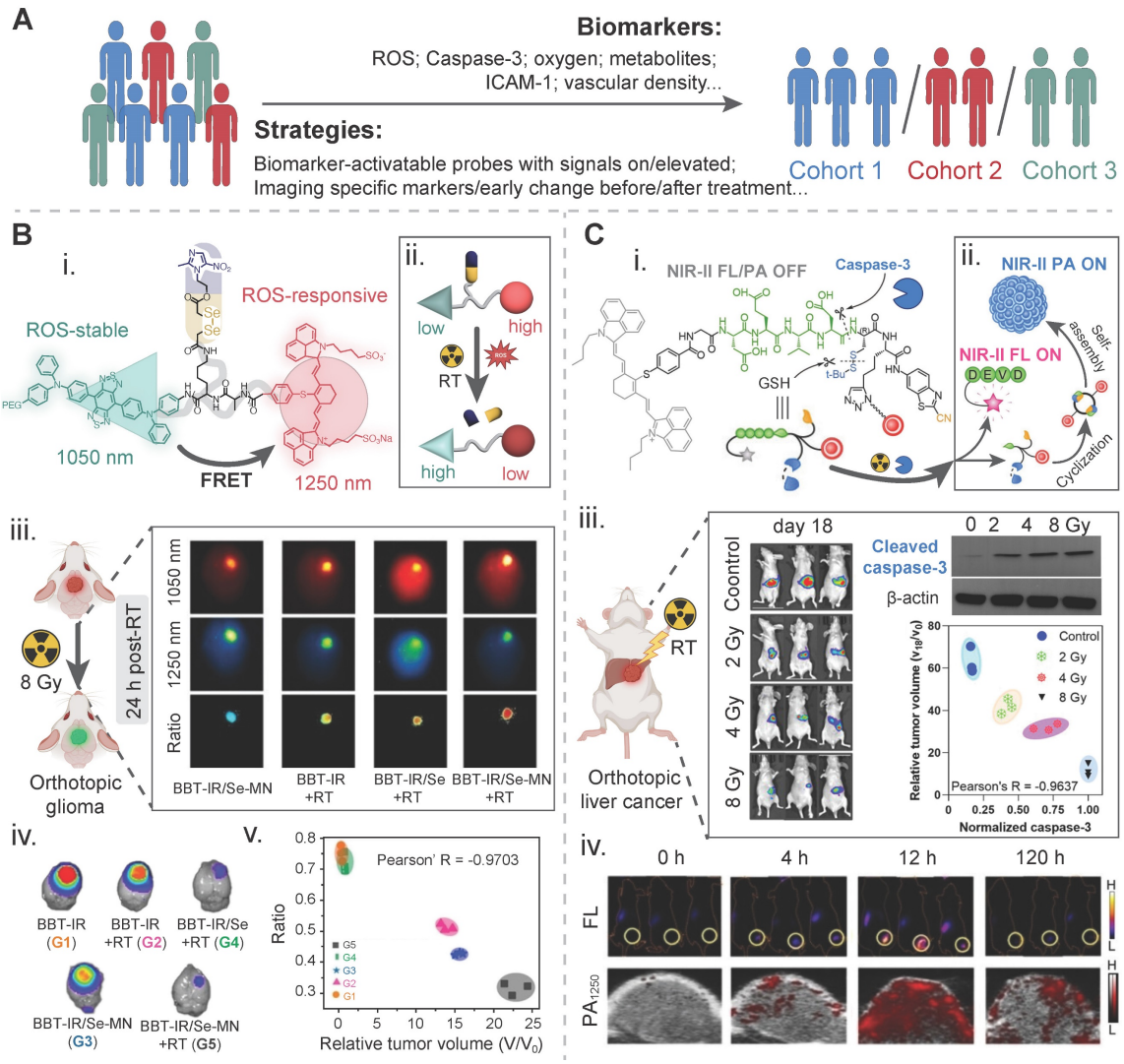

Figure 5. Biomarker-driven imaging probes for patient stratification. A) Illustration of strategies and biomarkers for radiotherapy stratification. B) A tumor reactive oxygen species (ROS)-activatable ratiometric fluorescent probe for reporting the ROS level during radiosensitizer-enhanced radiotherapy: (i) chemical structure and (ii) activatable mechanism of this nanoprobe; (iii) NIR-II FL images of orthotopic glioma-bearing mice in different treatment groups at 24 h post radiotherapy; (iv) bioluminescence images of the brain in the tumor model in different treatment groups on day 16 post radiotherapy. The intensity is an indicator of the tumor mass; (v) correlation between the ratiometric intensity and the relative tumor volume of these above groups on day 15 post radiotherapy. Adapted with permission [136]. Copyright 2023 WILEY-VCH GmbH. C) A caspase-3-activatable organic-inorganic hybrid nanoprobe for reporting the caspase-3 level during radiosensitizer-enhanced radiotherapy: (i) chemical structure and (ii) activatable mechanism of this nanoprobe. The red dot for a nanogapped gold nanoparticle; (iii) bioluminescence images of an orthotopic liver cancer model for measuring the tumor mass via the fluorescence intensity, western blotting images of activated caspase-3 in the tumor tissue, and the correlation between the caspase-3 level and the tumor mass in four treatment groups, i.e., the control (0 Gy), 2 Gy, 4 Gy, and 8 Gy; (iv) fluorescence images and photoacoustic images of ectopic xenograft HepG2 tumors under 8 Gy radiation at different time points after injection of the nanoprobe. Adapted with permission [134]. Copyright 2022 WILEY-VCH GmbH.

Photoacoustic imaging has recently emerged as a valuable tool to measure the level of tumor oxygenation [135]. To establish the correlation between photoacoustic lifetime-based oxygen images and γ-H2AX-stained histology results in a PDX breast cancer murine model after radiotherapy, an oxygen-sensing G2 polyacrylamide nanoparticle modified with a tumor-targeting F3 peptide, abbreviated as G2-PAA NPs, was injected into the tumor model to monitor the initial oxygen level and map its spatial distribution. After radiotherapy at a dose of 6 Gy was performed on a murine model, immunostaining of γ-H2AX in the resected tumor tissues was conducted. It was found that the local radiotherapy efficacy was positively correlated with the local oxygen level. However, concerns were raised on the calculation method for the structural similarity index with a low spatial resolution of PAI and the misalignment between some of these PAI images and their corresponding histology photos [132].

To enable early detection of radiotherapy-induced ROS, a ROS-responsive ratiometric imaging strategy is often applied because it has the advantage of avoiding false signal. A near-infrared ratiometric fluorescent and photoacoustic dual-model probe that was composed of an •OH-responsive chromophore diene electrochromic material (1-Br-Et), a dye NIR775, and IR1048. Ratiometric FL/PA imaging was

performed at twelve hours before and after three treatments on 4T1 tumor-bearing mice: (1) at a dose of 0 Gy, (2) at a dose of 10 Gy, and (3) at a dose of 10 Gy and with tempol as an •OH scavenger to obtain the baseline images and the post-therapy images, respectively. Compared to the baseline images, the normalized $\Delta FL_{780}/\Delta FL_{1113}$ value in the same tumor area treated with 10 Gy was declined by ~2.7-fold, while the normalized $\Delta PA_{755}/\Delta PA_{905}$ value was increased by ~1.4-fold. The changes in these values, particularly the $\Delta PA_{755}/\Delta PA_{905}$ value, could be diminished after the addition of tempol [133]. Another ratiometric NIR-II fluorescent molecular probe with a ROS-cleavable diselenide bond, termed BBT-IR/Se-MN, was developed for self-generation of ROS and self-monitoring of the ROS level. In this design, the Förster resonance energy transfer (FRET) between BBT, a ROS-insensitive donor-acceptor-donor fluorophore, and IR, a ROS-sensitive cyanine dye, was disrupted after the reaction of the probe with ROS, leading to a change in the ROS-responsive ratiometric optical signal. The signal intensity at 1050 nm for BBT was increased while the intensity at 1250 nm for IR declined. A negative correlation between the optical intensity ratios and the normalized relative tumor volumes, which corresponded to the early ROS level at 24 h after therapy and the final radiotherapeutic outcome, was established with a Pearson's R-value of -0.9703 in an orthotopic brain murine tumor model (**Figure 5B**) [136].

In vivo quantitative imaging of active caspase-3 within one day after radiation treatment could be used to reveal the early assessment result for the radiotherapy effect. A caspase-3-triggered nanoprobe, AuNNP@DEVD-IR1048, was developed by conjugating a NIR-II FL dye, IR-1048, to the surface of gold nanoparticles via a caspase-3 responsive peptide DEVD. It was found that the relative tumor volume (V_{18}/V_0, 18 and 0 for 18-day and 0-day after treatment) was a function of the normalized caspase-3 activity, as well as the intensity of ΔPA and ΔFL was a function of the relative tumor volume (V_{18}/V_0), respectively. Radiotherapy at three radiation doses of 2, 4, and 8 Gy was performed and non-irradiation one was set as a control, the Pearson's R value between V_{18}/V_0 and normalized caspase-3, ΔPA and V_{18}/V_0, and ΔFL and V_{18}/V_0 was calculated to be -0.9637, -0.9433, and -0.9577, respectively (**Figure 5C**) [134].

Overall, these studies have demonstrated the feasibility of using probes for early-phase imaging biomarkers, and there are correlations between early-phase imaging results and long-term therapeutic outcomes. In this context, patients whose biomarker expression is negative from initial imaging results could be classified into the non-responder group to radiotherapy and other treatment plans with better clinical benefits should be considered for them.

3.4. Imaging radiation-induced response: immune cell activity and beyond

To balance patients' risks and benefits, early determination of tumor response is conducive to continuing the current beneficial therapy, switching to an alternative therapy, or developing accurate population models due to tumor heterogeneity. Furthermore, with improved characterizations of the biological response of tumors to treatment methods, particularly, radiotherapy with immunomodulatory effects, advanced and efficacious therapeutic strategies might be developed. In clinical attempts and preclinical studies, several biological imaging techniques, such as diffusion kurtosis imaging [137], multi-parametric MRI [138], and highly sensitive whole-body PET/SPECT or optical imaging [139], have been trialed or tested to assess early tumor response to radiotherapy, concentrating on the level of cellular communities and acellular components.

Imaging immune cells and their activity. Specific surface receptors of immune cells and their secreted cytokines have been reported to be regulated during radiotherapy, and some of them have been correlated with therapeutic outcomes (**Figure 6A**) [86, 140-142]. In combination therapies with radiotherapy, imaging targets or biomarkers (e.g., surface receptors or secreted cytokines) for the T cell activity include programmed death-1 (PD-1), inducible T cell co-stimulator (ICOS), OX40, lymphocyte-activation gene 3 (LGA-3), T cell immunoglobulin and mucin domain-3 (TIM-3), granzyme B, interferon-gamma (IFN-γ), and interleukin-2 (IL-2). Biomarkers for the myeloid cells activity include CD40, CD206, colony-stimulating factor 1 receptor (CSF1R), C-C chemokine receptor 2 (CCR2), CD163, transforming growth factor beta (TGF-β), phosphatidylinositol 3-kinase gamma (PI3Kγ), and IL-12. In this context, nanoprobe hitchhike strategies/biomarker-targeted imaging strategies could be employed for imaging immune cells or monitoring their status/activity via a direct/indirect adherence manner (**Figure 6B**). Briefly, imaging probes can be attached onto immune cells or bound to secreted cytokines via receptor-ligand interaction for *in vivo* monitoring, and the biomarker expression, indicated by the intensity of imaging signals, can be correlated with the cell activity. In addition, longitudinal imaging of CAR T cells or other ACT cells via reporter genes or other methods provide additional insights into their biodistribution and tumor-infiltration, and the biological effect of radiotherapy in the era of cancer radio-immunotherapy [143, 144].

Per-fluoro-crown-ether (PFCE) nanoparticle-mediated ^{19}F MRI was explored to longitudinally monitor tumor-associated macrophages (TAMs) in glioma-bearing mice after radiotherapy and a radiotherapy recurrent gliomas model. The dynamics of TAM subpopulations were successfully monitored through MRI, while the NP uptake mechanism by different TAM phenotypes during the intervention of radiotherapy remained to be identified [145]. In addition to this novel imaging technique, conventional ^{1}H MRI and optical imaging approaches have been optimized and tuned for dynamic monitoring of TAMs during radiotherapy. For example, dynamic imaging of TAMs in response to low-dose radiotherapy (5 Gy) via a metabolizable dextran-indocyanine green NIR-II nanoprobe was conducted in SW1990 pancreatic tumor-bearing nude mice. The TAM-specific targeting was realized through the interaction of dextran in this probe with ICAM-3-grabbing nonintegrin-related 1 on TAMs. After three days post X-ray treatment, fluorescence images of the tumor area at different time points (6, 12, and 24 h) post-injection of the probe were recorded. A 2-fold increase in the signal intensity was found in the radiation-treatment group, compared to the non-treatment group and the TAM-depleting group [146]. Phenotypic polarization of macrophages during radiotherapy may be indirectly indicated with an elevated NO molecule level in the highly responsive tumor, thus the NO level could be used as a specific biomarker for TAM repolarization from the M2 to M1 phenotype. An ultrasmall paramagnetic iron oxide-based nanoprobe was modified and the aggregation of the nanoprobe could be triggered with an increase in the nitric oxide concentration. Comparing the treatment effects in a 4T1-tumor bearing murine model at three radiation doses (0 Gy, 0.5 Gy, and 3.0 Gy), a similar trend was observed for the ΔSNR_{tumor} in the T1 and T2 settings and the M1/M2 ratios in these groups: a significant change in the imaging contrast and an increase in the M1/M2 ratios in the 3.0 Gy-irradiated group compared to those in the non-treated group and the 0.5 Gy-treated group, while no statistical difference in both the imaging contrast and the M1/M2 ratio between the non-treated group and the 0.5 Gy-treated group (**Figure 6**C) [147].

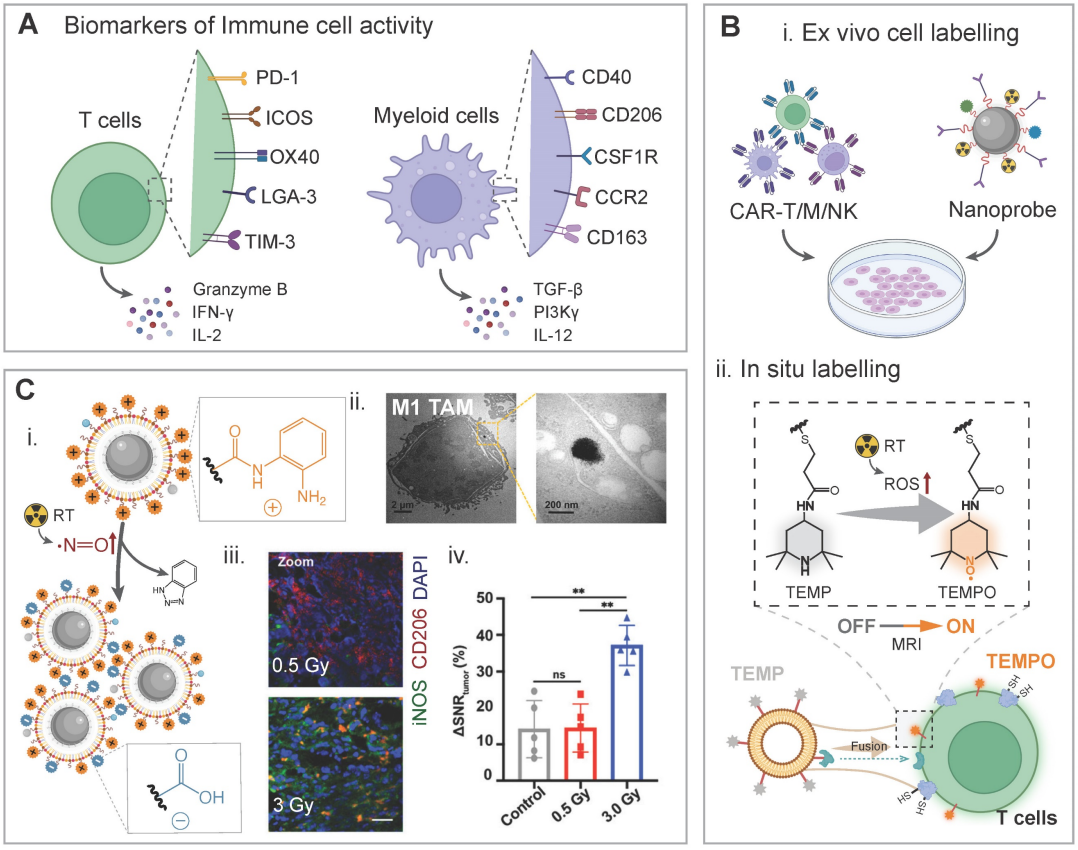

Figure 6. Biomarker-driven imaging probes for immune cells and their activities. A) Schematic illustration of biomarkers for immune cell activities during radiotherapy, including up/down-regulated surface receptors and secreted cytokines. B) Imaging of immune cells can be realized by ex vivo cell labelling and in situ labelling. Imaging-visible nanoprobes were ex vivo labelled with CAR-T/M/NK cells for real-time monitoring of their biodistribution, and T cell-directed liposomes were fused with T cell for in-situ labelling and they were activated when encountering radiation-induced ROS. C) Nitric oxide-triggered self-assembly of the USPIO@OMG nanoprobe for evaluating macrophage polarization during radiotherapy: (i) chemical principle for aggregation of the nanoprobe; (ii) TEM images to confirm the aggregation status of the nanoprobe in M1 macrophages; (iii) CLSM images of tumor slices from two radiation dose-treated groups, red CD206 signal indicates M2 macrophages while the green iNOS signal represents M1 macrophages; (iv) The T2 MRI signal changes in different groups. Adapted with permission [147]. Copyright 2023 American Chemical Society.

Other tumor-infiltrating immune cells have been imaged during radiotherapy. A circulating monocyte-hitchhike strategy was developed using a fluorescently labeled theranostic nanoprobe to monitor low-dose RT-facilitated monocyte chemotaxis. Mechanically, this nanoprobe could hitchhike RT-recruited monocytes via the interaction between its surface-modified lipoteichoic acid and the CD14 receptor on monocytes [148]. To specifically track tumor-infiltrating leukocytes (TILs), a series of "dual-locked" activatable near-infrared nanoprobes were developed. They were activated upon exposure to both leukocyte biomarkers (caspase-1, granzyme B, or neutrophil elastase) and the tumor biomarkers (aminopeptidase N). The selectivity of these nanoprobes towards specific biomarkers was verified both *in vitro* and *in vivo*. More importantly, these nanoprobes could differentiate subpopulations of TILs, and they could be employed for patient stratification and therapeutic efficacy prediction [149].

Imaging hypoxia. Probes have also been developed to monitor the hypoxic dynamics (magnitude and distribution) to evaluate the level of tumor reoxygenation in the tumor during radiotherapy. It was revealed by a near-infrared phosphorescent nanoprobe, consisting of a fluorescent semiconducting polymer and a palladium complex, that a higher fractional dose (10 Gy × 3 f) was more effective in improving tumor reoxygenation in a Hela tumor (diameter: 8 mm)-bearing nude murine model than a lower dose (2 Gy) [150]. Another phosphorescent probe with Cherenkov-excited luminescence imaging properties, Oxyphor PtG4, was developed to image pO_2 distribution during radiotherapy. After analyzing the obtained pO_2 images with various spatial resolutions in the range of 0.2 mm to 5 mm, it was found the hypoxic fractions was decreased by more than 50% after radiotherapy at a dose of 5 Gy × 5 f on MDA-MB-231 or FaDu tumor-bearing murine models, or 8 Gy on MDA-MB-231 tumor models, and accurate imaging was realized by images with a high spatial resolution of 0.2 mm [151].

Imaging the redox status. A radiation-induced ROS-activatable disassembled nanoprobe was constructed from a PEG-PPS-PEG-NH2 polymer, iron oxide nanoparticles (IO NPs), and DOTA-Gd. In this design, radiation-induced ROS-responsive "turn-on" of the T1 signal was achieved through the disassembly of the nanoprobe via the oxidation of hydrophobic thioethers to hydrophilic sulfones and an increased distance between IO NPs as a quencher and DOTA-Gd as an enhancer. A high Pearson's correlation coefficient was observed between changes in the T_1 signal changes at 24-48 h post-treatment and the frequency of $CD4^+CD8^+$ T cells as an indicator for adaptive immunity (R = 0.9831) or the tumor inhibition rate (R = 0.9308) after radiotherapy. Therefore, this nanoprobe could be employed for early and accurate evaluation of radiotherapeutic treatment outcomes at 24-48 h post-treatment [10].

Imaging caspase-3. A caspase-3-activated probe with "turn-on" fluoro-photoacoustic signal was developed for early evaluation of the external radiotherapy effect. Self-assembly of this probe was triggered under the stimulation of upregulated caspase-3 induced by radiotherapy and significant changes in the fluorescence intensity and the photoacoustic intensity were detected. In an EL4 lymphoma tumor-bearing murine model treated with a range of radiation doses (i.e., 0, 1, 2, 5, 10 Gy), the normalized fluorescent intensities and ΔPA signal intensities were positively correlated with the radiation doses at 3-24 h post *i.v.* injection of the probe. Furthermore, they were negatively correlated with the relative tumor size on day 21 post-radiotherapy with a high Pearson's R-value of -0.8989 and -0.9428, respectively, implying that a stronger signal enhancement at the tumor sites after radiotherapy may be used to predict a smaller tumor size after radiotherapy [152]. A PSMA-targeted, ^{177}Lu-labeled theranostic probe conjugated with a hemicyanine-based NIR agent via a DEVD peptide cleaved by caspase-3 was prepared for fluorescence imaging to assess the elevated level of internal radiotherapy-induced caspase-3. Statistically, this theranostic probe had a low K_i value of 4.12 nM and a low K_m value of 67.62 μM, suggesting it had strong binding affinity to PSMA. The detection of limitation was down to 0.125 U/ml of caspase-3 which was derived from the fluorescence signal. Therefore, it was very sensitive to changes in caspase-3. In a medium PSMA-expressing 22Rv1 prostate cancer model, this probe achieved a 1.79-fold fluorescence contrast enhancement [153].

Taken together, conventional fMRI scanning approaches and other quantitative imaging modalities have already been used to monitor the biological response in the tumor during the treatment procedure for external/internal radiotherapy [125, 154]. These quantitative imaging modalities also lay a solid foundation for developing biomarkers-driven molecular imaging with specificity and accuracy. After radiation-associated biomarkers have been experimentally identified or preliminarily validated from gene, RNA, and protein analysis, specific imaging probes targeting these biomarkers could be prepared, and quantitative imaging modalities are then applied to image these molecular biomarkers.

3.5. Predicting toxicity potential and resistance

Radiotherapy-induced adverse effects have been reported, including brain injury [155], radiation dermatitis [156], bone loss, radiation-induced intestinal fibrosis (RIF) [157], and radiation-induced acquired therapy resistance. The success or failure of a therapy would be heavily relied on these adverse effects. Conventionally, treatment (e.g., radiation)-induced adverse events are graded according to the Common Terminology Criteria for Adverse Events (CTCAE v.5.0). Imaging techniques based on toxicity- or resistance-associated biomarkers could provide an alternative non-invasive, spatiotemporal, and objective assessment approach to implementing these criteria for assessing radiation-induced adverse effects. Meanwhile, advanced imaging processing tools, particularly machine learning and artificial intelligence, may play a crucial role in predicting treatment failure and RT-induced toxicities [158].

In general, excess ROS generated after radiation accounts for the principal source of radiation-induced toxicity (e.g., acute esophagitis and vasculitis.) [11, 159, 160]. Hypoxia, therapy-induced senescence, and resistant cellular types are the predominant contributors for radioresistance. Accurate and timely elucidation of normal tissue injury and tumor tissue radioresistance using these biomarkers-driven imaging probes in an non-invasive and spatiotemporal manner is conducive to risk stratification, early intervention, and re-optimization of treatment plans.

Radiation-induced lung injury (RILI). It has been reported that the majority of radiation pneumonitis occurs within 4-12 weeks after completion of radiation therapy [161, 162]. In light of steroids intervention has a good therapeutic effect on radiation pneumonitis at its early phase, the biomarkers for early detection are essential to improve the patient outcomes. An earlier marker, i.e., C-X-C-chemokine-receptor-type-4 (CXCR4), was explored for diagnosis with the aid of a CXCR4-targeted PET probe, [^{18}F]AlF-NOTA-QHY-04. A RILI rat model and a large population of 14 patients with radiation pneumonia were included in this study. A remarkably higher peak of the imaging signal was observed in the irradiated lung tissue than the unirradiated one on day 14 post-radiotherapy in rat models, and cancer patients with grade-2 RILI exhibited a significantly higher SUVmax value than those with grade-1 RILI [163]. To allow specific evaluation of radiation-induced lung fibrosis, an integrin αvβ6-targeted PET probe, [^{18}F]-FBA-A20FMDV2, was used in an imaging study. Six non-small cell lung cancer patients after radiotherapy and six healthy volunteers were included in this study. A higher mean PET uptake of probes was observed in the irradiated lung compared with the healthy control (2.97 vs 1.99, $p < 0.05$). Furthermore, there was a remarkable pharmacodynamic relationship between the uptake level of the integrin-targeted tracer and the radiation dose [164]. This preliminary study suggests that integrin αvβ6 could be used as an imaging target for radiation-induced lung fibrosis. Two trials have confirmed the feasibility of using type 1 collagen as a RILI biomarker (NCT04485286 and NCT03535545). In both trials, two distinctive type 1 collagen-targeted probes, a MR probe, EP-3533, and a PET probe, ^{68}Ga-GBP8, were applied to image the developed murine model after lung radiation, as well as excised human lung tissues with RILI from six human subjects. The imaging signal intensity was well correlated with the severity degree of progressive fibrosis, indicated by the collagen proportional area in excised tissues, and the RILI area in human subjects [165].

Radiation-induced myocardial damage. One should note that radiation even at a low dose might cause toxicity, such as a risk of heart diseases [166]. Coronary artery calcium (CAC) scores [167], serum lipopolysaccharide-binding proteins [168], and the MRI-derived extracellular volume are set as prognostic risk factors for adverse cardiac events after thoracic radiotherapy.

For imaging radiation-induced cardiotoxicity (e.g., cardiac remodeling and fibrosis), several potential targets could be used, such as somatostatin receptors, αvβ3 integrin receptor, fibroblast activation protein (FAP), norepinephrine transporter, mitochondrial membrane potential, and ROS [169-171]. In a retrospective study of 32 cancer patients undergoing ^{68}Ga-labeled FAPI PET examination, myocardial uptake of these tracers was found to be associated with coronary artery disease (CAD), age, and left ventricular ejection fraction (LVEF), indicating these parameters could be considered in early risk stratification [172]. Early detection of radiation-induced myocardial damage using ^{18}F-AlF-NOTA-FAPI-04 PET/CT imaging can be realized before a decrease in left ventricular ejection fraction. Specifically, in rat models, the myocardial FAPI uptake was significantly increased at 2nd week and peaked at 5th week post-radiation, whereas the LVEF was dramatically declined at 8th week [173].

Several serum biomarkers and urine biomarkers have been evaluated for early and accurate assessment of radiation-induced toxicity [168, 174,

175], but failed to locate the toxicity origins. To this end, early imaging biomarkers for a specific manifestation are actively screened to achieve monitoring of a spatiotemporal toxicity profile.

Radioresistance. To accurately profile the degree of radioresistance is essential for reaching treatment decisions. As galectins are positively correlated with the hypoxia level, a ^{68}Ga-galectracer PET probe, ^{68}Ga-NOTA-PEG4-TDGd, was constructed by radiolabeling a thiodigalactoside derivative to explore its prediction capacity of radioresistance. This prediction capacity was confirmed in a 4T1-bearing mice model, and a higher tumor uptake of the galectin-targeted tracer was associated with significantly poorer tumor response to radiotherapy [176]. Cancer-associated fibroblasts (CAFs) constitute nearly 90% of the whole tumor volume in epithelial tumors, and they play a crucial role in mediating radio-resistance [177]. It is noted that the fibroblast activation protein is a valuable biomarker for CAFs. Prior to the construction of targeted imaging probes for the well-defined biomarker, effective FAPI ligands, including FAPI-46, FAPI-46-F1D, FAPI-46-EB, FAPI-46-Ibu, FAP-2286, have been developed [178]. In addition, transforming growth factor β (TGF β), a therapeutically negative factor, could be a targetable imaging marker during radiotherapy. A TGF β neutralizing mAb was radiolabeled with PET radionuclide ^{89}Zr to form ^{89}Zr-fresolimumab and it was then applied to image radiation-induced TGF β activation. To screen active TGF β expression from tumor slices and the tumor radioactivity from *in vivo* PET-CT images, comparisons were made between the active and latent TGF β status in two cell lines (C19 and B9), as well as between the αvβ8-positive and αvβ8-negative Lewis lung carcinoma (LLC). It was confirmed that ^{89}Zr-fresolimumab could actively and specifically image TGF β activation. This probe-mediated PET imaging and four treatments (sham, 1D11 as a TGF β inhibitor, RT, and RT + 1D11) were performed on three distinctive intracranial tumor models, including two murine glioblastomas (GL261 and SB28) and one brain-adapted 4T1 murine breast cancer. To note, 1D11 exhibited a similar survival curve as the sham group, while the combination of RT with 1D11 significantly extended the survival rate compared to other groups. These extended benefits were found to be correlated with the level of TGFβ activity detected by PET imaging [179].

However, these novel potential biomarkers for radiotherapy imaging are identified and validated from multiple cohorts of clinical trials or practices, and their clinical values remain to be verified. These biomarker pools are critical for future implementation of personalized radiotherapy.

4. Reflection and future perspective

Five phases are usually involved in the development of biomarkers: preclinical exploratory, clinical assay and validation, retrospective longitudinal monitoring, prospective screening, and cancer control [180]. Through these steps, potential biomarkers have been reported in preclinical and clinical trials, while these biomarkers await robust validation and accurate qualification, and only those associated with clinical outcomes could be considered for clinical use. It is expected that biomarker-driven molecular imaging could provide crucial information to make 'go or no-go' decision after identification of treatment failure at an early stage so that side effects could be avoided for patients. Meanwhile, positive outcomes from imaging biomarkers at the early stage of treatment may act as indicators for surrogate clinical endpoints of successful treatment.

Humanized patient-derived xenografts mouse models are preferred for identifying and validating radiotherapy-specific biological or radiological biomarkers [181-183]. The accurate tumor-specific anatomic information and dynamic multi-modality/multi-parametric functional images from biomarker-driven probe-mediated molecular imaging could provide a large and reliable training source for the development of advanced imaging processing tools, such as machine learning and artificial intelligence [184]. In clinical trials, the imaging evaluation system needs to consider these parameters: the eligibility criteria, endpoints, trial feasibility, as well as interobserver variabilities in the tumor size measurement. In this context, predictive biomarkers instead of prognostic ones could be explored to pre-determine the endpoint of clinical trials [185]. In addition, new potent endpoints, for instance, growth modulation index (GMI), could be incorporated into the imaging evaluation system.

Reflection and future perspectives of developing imaging biomarkers and biomarker-driven molecular imaging probes in radiotherapy are provided after we carefully review previous successes and failures of clinical and preclinical studies.

I. Technical and clinical validations of biological imaging biomarkers are currently very active. Unfortunately, the majority of them fail during their translation into a medical research tool, and significantly challenging issues lie in their translation into a decision-making tool, because of their low screening, diagnostic, or predictive valence [23]. Thus, at the first beginning, imaging biomarker candidates, particularly molecular biomarkers, should be obtained from a robust procedure of identification

and validation using multiple molecular techniques, such as cDNA microarray analysis, clone sequencing, oligonucleotide arrays, reverse-phase protein lysate arrays, and tissue microarrays. In this context, the defined molecular biomarkers and their correlations with clinical benefits can have a solid biological basis. False/negative/positive imaging signal resulting from chemical, biological, or structural changes of biomarkers, especially the enzyme, could be avoided.

II. It is of utmost importance to reveal typical response patterns or biological alternations induced by various radiotherapy modalities/sources and different combinational radiation therapies in cancer patients or clinical samples. These findings can therefore provide the guidelines of predicting long-term clinical outcomes and radiation-induced side effects, and accelerate clinical use of beneficial combinational radiotherapy. Critically, evaluation of these novel molecular imaging biomarkers should be conducted in a larger patient cohort. Additionally, in agreement with one of the recommendations proposed by the Consensus Statement [23], all true-negative, false-negative, and false-positive data obtained from these exploratory studies on either animals or humans should be published or shared in a public database.

III. As radiopharmaceutical therapy (RPT) has been expected to be the mainstream of radiation oncology practice, its differences from external beam radiotherapy (EBRT) in dosing rates and dose distributions may lead to unexpected treatment response and toxicities. The major concern will be patient-specific dosimetry in treatment planning [186]. Biomarker-targeted imaging probes could be explored to provide critical information on the receptor phenotype and its expression level, as well as its binding sites, which helps bridging the knowledge gap in revealing the differences between RPT and EBRT. In addition, during translation of preclinical results into clinical trials, one should note that the receptor phenotype and expression can vary significantly between human models and rodent/murine tumor models before, during, after radiation therapy [187]. Pharmacodynamics biomarkers and special imaging effects, such as the tumor sink effect in large-tumor-bearing patients, should also be considered when interpreting imaging results.

IV. Specific and adequate accumulation of probes for imaging radiotherapy in the area of interest with robust imaging enhancements and a great safety profile should be addressed during the design step. In this context, from a chemical structure perspective, the ligands for targeting biomarkers [178], the linkers cleavable by biomarkers [188, 189], the chelators for paramagnetic ions or diagnostic radionuclides [190], and the biomarker-activatable imaging enhancement principles should be considered for the probes [191]. The basic *in vivo* working mechanism(s) of a certain probe type, including tumor targeting [192], excretion [193], and signal activation [14], should become the cornerstone for the development of probe-mediated molecular imaging. Novel nanoprobes from the same nanoprobe type could help shortening their development time, while their preclinical and clinical data could continuously and dynamically mature the mechanism(s) of this nanoprobe type.

V. In the roadmap of biomarker-driven imaging probes towards clinical translation, consensus guidelines on their synthesis methods and performance of biological imaging-guided adaptive radiotherapy are essential to reduce the bias or variability between interobservers, inter-institutions or intra-institutions [194]. In addition, instrumental contributions are fundamental to improve radiotherapy planning, including synthetic computed tomography for MRI online adaptive planning [195] and optimization of imaging reconstruction algorithms in dosimetry [196]. In the era of precision radiotherapy, the use of advanced techniques such as artificial intelligence (AI) and machine learning (ML) is on the rise [197]. The radiomics features with quantitative metrics (texture, morphology, and dosimetry) extracted from imaging modalities such as PET or MRI are abundant and they could be explored to assess biological, physiological, metabolic changes before, during and after radiotherapy, such as identifying the T cell exhaustion status [198] and predicting pathological complete response of neoadjuvant radiotherapy [199].

5. Concluding remarks

Individual biological targets are the foundation of personalized radiotherapy. Imaging biomarkers at genetic, proteomic, and metabolomic levels can provide informative guidance for radiotherapy interventions. Thus, comprehensive spatiotemporal imaging of molecular biomarkers and quantitative analysis of these radiomics features help achieving better cancer management. Although imaging biomarkers have been widely explored and assessed, evaluations of them has not been conducted in a large patient cohort. Very few biological biomarkers that are well correlated with radiotherapeutic outcomes including clinical benefits and side effects have been identified and verified. Collaborative efforts should be made into building the correlations of imaging biomarkers with biological and pathological changes, tumor growth control degrees, side effects to normal tissues before, during and after radiotherapy or combined radiotherapy. It will be equally important

to develop nanoprobes for these imaging biomarkers which can be readily translated from rodent/murine tumor models to human subjects.

Abbreviations

ADC: apparent diffusion coefficient; AIE: aggregation-induced emission; BOLD: blood-oxygen-level-dependent; BTV: biological target volume; CAFs: cancer-associated fibroblasts; CEST: chemical exchange saturation transfer; CSCs: cancer stem cells; CT: computed tomography; CTV: clinical target volume; EBRT: external beam radiation therapy; EGFR: epidermal growth factor receptor; EPRI: electron paramagnetic resonance imaging; FAP: fibroblast activation protein; FL: fluorescence; FRET: fluorescence resonance energy transfer; GTV: gross tumor target volume; HPV: human papillomavirus; ICAM-1: intracellular adhesion molecule-1; ICT: intramolecular charge transfer; IGF-1R: insulin-like growth factor 1 receptor; LVEF: left ventricular ejection fraction; MRI: magnetic resonance imaging; mpMRI: multiparametric magnetic resonance imaging; MRS: magnetic resonance spectroscopy; OS: overall survival; PAI: photoacoustic imaging; PET: positron emission tomography; PFS: progression-free survival; pO_2: oxygen partial pressure; RPT: radiopharmaceutical therapy; PSMA: prostate-specific membrane antigen; PTV: planning target volume; RILI: radiation-induced lung injury; RECIST: Response Evaluation Criteria in Solid tumours; ROS: reactive oxygen species; SPECT: single photon emission computed tomography; SUV: standard uptake value; TAMs: tumor-associated macrophages; TGF β: transforming growth factor β; TILs: tumor-infiltrating leukocytes; TLG: total lesion glycolysis.

Acknowledgements

Graphic Abstract and Illustrations were created with Adobe Illustrator and/or BioRender.com. This work was financially supported by the National Natural Science Foundation of China (52073193, 51873120, 81621003), the Sichuan Provincial Department of Science and Technology Project (2024NSFJQ0050), and the 1·3·5 Project for Disciplines of Excellence, West China Hospital, Sichuan University (ZYJC21013).

Author contributions

H.-N. Li and K. Luo conceived the outline of this review. H.-N. Li collected papers for writing, drafted the original manuscript, and performed the creation of figures/tables. Q.-Y. G helped revise the manuscript and discuss the content. K. Luo supervised this project and finalized this manuscript. All authors have read and approved the final manuscript.

Competing Interests

The authors have declared that no competing interest exists.

References

1. Olin AB, Hansen AE, Rasmussen JH, Ladefoged CN, Berthelsen AK, Håkansson K, et al. Feasibility of multiparametric positron emission tomography/magnetic resonance imaging as a one-stop shop for radiation therapy planning for patients with head and neck cancer. Int J Radiat Oncol Biol Phys. 2020; 108: 1329-38.
2. Vitzthum LK, Surucu M, Gensheimer MF, Kovalchuk N, Han B, Pham D, et al. BIOGUIDE-X: a first-in-human study of the performance of positron emission tomography-guided radiation therapy. Int J Radiat Oncol Biol Phys. 2024; 118:1172-80.
3. Michaelis LC, Ratain MJ. Measuring response in a post-RECIST world: from black and white to shades of grey. Nat Rev Cancer. 2006; 6: 409-14.
4. Gafita A, Djaileb L, Rauscher I, Fendler WP, Hadaschik B, Rowe SP, et al. Response Evaluation Criteria in PSMA PET/CT (RECIP 1.0) in metastatic castration-resistant prostate cancer. Radiology. 2023; 308: 222148.
5. Li H, Luo Q, Zhang H, Ma X, Gu Z, Gong Q, Luo K. Nanomedicine embraces cancer radio-immunotherapy: mechanism, design, recent advances, and clinical translation. Chem Soc Rev. 2023; 52: 47-96.
6. Pan Y, Tang W, Fan W, Zhang J, Chen X. Development of nanotechnology-mediated precision radiotherapy for anti-metastasis and radioprotection. Chem Soc Rev. 2022; 51: 9759-830.
7. Gerwing M, Herrmann K, Helfen A, Schliemann C, Berdel WE, Eisenblätter M, Wildgruber M. The beginning of the end for conventional RECIST - novel therapies require novel imaging approaches. Nat Rev Clin Oncol. 2019; 16: 442-58.
8. Adebahr S, Althaus A, Scharl S, Strouthos I, Farolfi A, Serani F, et al. The prognostic significance of a negative PSMA-PET scan prior to salvage radiotherapy following radical prostatectomy. Eur J Nucl Med Mol Imaging. 2024; 51: 558-67.
9. Lee SCS, Pyo AHA, Koritzinsky M. Longitudinal dynamics of the tumor hypoxia response: from enzyme activity to biological phenotype. Sci Adv. 2023; 9: eadj6409.
10. Zhou Z, Deng H, Yang W, Wang Z, Lin L, Munasinghe J, et al. Early stratification of radiotherapy response by activatable inflammation magnetic resonance imaging. Nat Commun. 2020; 11: 3032.
11. Babu B, Pawar S, Mittal A, Kolanthai E, Neal CJ, Coathup M, Seal S. Nanotechnology enabled radioprotectants to reduce space radiation-induced reactive oxidative species. Wiley Interdiscip Rev Nanomed Nanobiotechnol. 2023; 15: 1896.
12. Vollenbrock SE, Voncken FEM, Lambregts DMJ, Maas M, Donswijk ML, Vegt E, et al. Clinical response assessment on DW-MRI compared with FDG-PET/CT after neoadjuvant chemoradiotherapy in patients with oesophageal cancer. Eur J Nucl Med Mol Imaging. 2021; 48: 176-85.
13. Grambozov B, Kalantari F, Beheshti M, Stana M, Karner J, Ruznic E, et al. Pretreatment 18-FDG-PET/CT parameters can serve as prognostic imaging biomarkers in recurrent NSCLC patients treated with reirradiation-chemoimmunotherapy. Radiother Oncol. 2023; 185: 109728.
14. Ma X, Mao M, He J, Liang C, Xie HY. Nanoprobe-based molecular imaging for tumor stratification. Chem Soc Rev. 2023; 52: 6447-96.
15. Hsu JC, Tang Z, Eremina OE, Sofias AM, Lammers T, Lovell JF, et al. Nanomaterial-based contrast agents. Nat Rev Methods Primers. 2023; 3: 30.
16. Pallares RM, Mottaghy FM, Schulz V, Kiessling F, Lammers T. Nanoparticle diagnostics and theranostics in the clinic. J Nucl Med. 2022; 63: 1802-8.
17. Liu Q, Zou J, Chen Z, He W, Wu W. Current research trends of nanomedicines. Acta Pharm Sin B. 2023; 13: 4391-416.
18. Group F-NBW. BEST (Biomarkers, EndpointS, and other Tools) Resource. Silver Spring (MD): Food and Drug Administration (US); 2016.
19. Sellmyer MA, Lee IK, Mankoff DA. Building the bridge: molecular imaging biomarkers for 21(st) century cancer therapies. J Nucl Med. 2021; 62: 1672-6.
20. Barker HE, Paget JT, Khan AA, Harrington KJ. The tumour microenvironment after radiotherapy: mechanisms of resistance and recurrence. Nat Rev Cancer. 2015; 15: 409-25.
21. Pallud J, Llitjos JF, Dhermain F, Varlet P, Dezamis E, Devaux B, et al. Dynamic imaging response following radiation therapy predicts long-term outcomes for diffuse low-grade gliomas. Neuro Oncol. 2012; 14: 496-505.
22. Read GH, Bailleul J, Vlashi E, Kesarwala AH. Metabolic response to radiation therapy in cancer. Mol Carcinog. 2022; 61: 200-24.
23. O'Connor JP, Aboagye EO, Adams JE, Aerts HJ, Barrington SF, Beer AJ, et al. Imaging biomarker roadmap for cancer studies. Nat Rev Clin Oncol. 2017; 14: 169-86.
24. Chen WC, Choudhury A, Youngblood MW, Polley MC, Lucas CG, Mirchia K, et al. Targeted gene expression profiling predicts meningioma outcomes and radiotherapy responses. Nat Med. 2023; 29: 3067-76.

25. Pellerin A, Khalifé M, Sanson M, Rozenblum-Beddok L, Bertaux M, Soret M, et al. Simultaneously acquired PET and ASL imaging biomarkers may be helpful in differentiating progression from pseudo-progression in treated gliomas. Eur Radiol. 2021; 31: 7395-405.
26. Galldiks N, Niyazi M, Grosu AL, Kocher M, Langen KJ, Law I, et al. Contribution of PET imaging to radiotherapy planning and monitoring in glioma patients - a report of the PET/RANO group. Neuro Oncol. 2021; 23: 881-93.
27. Choi W, Park B, Choi S, Oh D, Kim J, Kim C. Recent advances in contrast-enhanced photoacoustic imaging: overcoming the physical and practical challenges. Chem Rev. 2023; 123: 7379-419.
28. Horsman MR, Mortensen LS, Petersen JB, Busk M, Overgaard J. Imaging hypoxia to improve radiotherapy outcome. Nat Rev Clin Oncol. 2012; 9: 674-87.
29. Xie F, Wei W. [(64)Cu]Cu-ATSM: an emerging theranostic agent for cancer and neuroinflammation. Eur J Nucl Med Mol Imaging. 2022; 49: 3964-72.
30. Vats K, Mallia MB, Mathur A, Sarma HD, Banerjee S. '4+ 1'Mixed ligand strategy for the preparation of 99mTc-radiopharmaceuticals for hypoxia detecting applications. ChemistrySelect. 2017; 2: 2910-6.
31. Jans HS, Stypinski D, Mcquarrie S, Kumar P, Mercer J, Wiebe L, McEwan S. SU-E-CAMPUS-I-03: dosimetric comparison of the hypoxia agent iodoazomycin arabinoside (IAZA) labeled with the radioisotopes I-123, I-131 and I-124. Med Phys. 2014; 41: 385.
32. A R, Wang H, Nie C, Han Z, Zhou M, Atinuke OO, et al. Glycerol-weighted chemical exchange saturation transfer nanoprobes allow (19)F(/1)H dual-modality magnetic resonance imaging-guided cancer radiotherapy. Nat Commun. 2023; 14: 6644.
33. Kishimoto S, Devasahayam N, Chandramouli GVR, Murugesan R, Otowa Y, Yamashita K, et al. Evaluation of a deuterated triarylmethyl spin probe for in vivo R(2) ⁎-based EPR oximetric imaging with enhanced dynamic range. Magn Reson Med. 2024; 91: 413-23.
34. Cui S, Pratx G. 3D computational model of oxygen depletion kinetics in brain vasculature during FLASH RT and its implications for in vivo oximetry experiments. Med Phys. 2022; 49: 3914-25.
35. García-Figueiras R, Baleato-González S, Luna A, Padhani AR, Vilanova JC, Carballo-Castro AM, et al. How imaging advances are defining the future of precision radiation therapy. Radiographics. 2024; 44: 230152.
36. Ai D, Hao S, Shen W, Wu Q, Zhang S, Chen Y, et al. Induction sintilimab and chemotherapy followed by concurrent chemoradiotherapy for locally advanced esophageal cancer: a proof-of-concept, single-arm, multicenter, phase 2 trial. EClinicalMedicine. 2024; 69: 102471.
37. Arai TJ, Yang DM, Campbell JW, 3rd, Chiu T, Cheng X, Stojadinovic S, et al. Oxygen-sensitive MRI: a predictive imaging biomarker for tumor radiation response? Int J Radiat Oncol Biol Phys. 2021; 110: 1519-29.
38. Lin L, Wang LV. The emerging role of photoacoustic imaging in clinical oncology. Nat Rev Clin Oncol. 2022; 19: 365-84.
39. Hesse F, Wright AJ, Somai V, Bulat F, Kreis F, Brindle KM. Imaging glioblastoma response to radiotherapy using 2H magnetic resonance spectroscopy measurements of fumarate metabolism. Cancer Res. 2022; 82: 3622-33.
40. Bisgaard ALH, Brink C, Fransen ML, Schytte T, Behrens CP, Vogelius I, et al. Robust extraction of biological information from diffusion-weighted magnetic resonance imaging during radiotherapy using semi-automatic delineation. Phys Imaging Radiat Oncol. 2022; 21: 146-52.
41. Fang P, Musall BC, Son JB, Moreno AC, Hobbs BP, Carter BW, et al. Multimodal imaging of pathologic response to chemoradiation in esophageal cancer. Int J Radiat Oncol Biol Phys. 2018; 102: 996-1001.
42. Jung M, Bogner B, Diallo TD, Kim S, Arnold P, Füllgraf H, et al. Multiparametric magnetic resonance imaging for radiation therapy response monitoring in soft tissue sarcomas: a histology and MRI co-registration algorithm. Theranostics. 2023; 13: 1594-606.
43. Mohamed ASR, Abusaif A, He R, Wahid KA, Salama V, Youssef S, et al. Prospective validation of diffusion-weighted MRI as a biomarker of tumor response and oncologic outcomes in head and neck cancer: results from an observational biomarker pre-qualification study. Radiother Oncol. 2023; 183: 109641.
44. Onal C, Erbay G, Oymak E, Guler OC. The impact of the apparent diffusion coefficient for the early prediction of the treatment response after definitive radiotherapy in prostate cancer patients. Radiother Oncol. 2023; 184: 109677.
45. Mowery YM, Vergalasova I, Rushing CN, Choudhury KR, Niedzwiecki D, Wu Q, et al. Early (18)F-FDG-PET response during radiation therapy for HPV-related oropharyngeal cancer may predict disease recurrence. Int J Radiat Oncol Biol Phys. 2020; 108: 969-76.
46. Qin H, Zhang V, Bok RA, Santos RD, Cunha JA, Hsu IC, et al. Simultaneous metabolic and perfusion imaging using hyperpolarized (13)C MRI can evaluate early and dose-dependent response to radiation therapy in a prostate cancer mouse model. Int J Radiat Oncol Biol Phys. 2020; 107: 887-96.
47. Nozaki S, Nakatani Y, Mawatari A, Shibata N, Hume WE, Hayashinaka E, et al. Comparison of [18F]FIMP, [11C]MET, and [18F]FDG PET for early-phase assessment of radiotherapy response. Sci Rep. 2023; 13: 1961.
48. Rosar F, Wenner F, Khreish F, Dewes S, Wagenpfeil G, Hoffmann MA, et al. Early molecular imaging response assessment based on determination of total viable tumor burden in [(68)Ga]Ga-PSMA-11 PET/CT independently predicts overall survival in [(177)Lu]Lu-PSMA-617 radioligand therapy. Eur J Nucl Med Mol Imaging. 2022; 49: 1584-94.
49. Peltier A, Seban RD, Buvat I, Bidard FC, Mechta-Grigoriou F. Fibroblast heterogeneity in solid tumors: from single cell analysis to whole-body imaging. Semin Cancer Biol. 2022; 86: 262-72.
50. Wang B, Liu W, Liu C, Du K, Guo Z, Zhang G, et al. Cancer-associated fibroblasts promote radioresistance of breast cancer cells via the HGF/c-Met signaling pathway. Int J Radiat Oncol Biol Phys. 2023; 116: 640-54.
51. Hu K, Ma X, Xie L, Zhang Y, Hanyu M, Obata H, et al. Development of a stable peptide-based PET tracer for detecting CD133-expressing cancer cells. ACS Omega. 2022; 7: 334-41.
52. Baumann M, Krause M, Overgaard J, Debus J, Bentzen SM, Daartz J, et al. Radiation oncology in the era of precision medicine. Nat Rev Cancer. 2016; 16: 234-49.
53. Krause M, Yaromina A, Eicheler W, Koch U, Baumann M. Cancer stem cells: targets and potential biomarkers for radiotherapy. Clin Cancer Res. 2011; 17: 7224-9.
54. Deng L, Liang H, Burnette B, Beckett M, Darga T, Weichselbaum RR, Fu YX. Irradiation and anti-PD-L1 treatment synergistically promote antitumor immunity in mice. J Clin Invest. 2014; 124: 687-95.
55. Kunihiro AG, Sarrett SM, Lastwika KJ, Solan JL, Pisarenko T, Keinänen O, et al. CD133 as a biomarker for an autoantibody-to-ImmunoPET paradigm for the early detection of small cell lung cancer. J Nucl Med. 2022; 63: 1701-7.
56. Rashidian M, LaFleur MW, Verschoor VL, Dongre A, Zhang Y, Nguyen TH, et al. Immuno-PET identifies the myeloid compartment as a key contributor to the outcome of the antitumor response under PD-1 blockade. Proc Natl Acad Sci U S A. 2019; 116: 16971-80.
57. Nigam S, McCarl L, Kumar R, Edinger RS, Kurland BF, Anderson CJ, et al. Preclinical ImmunoPET imaging of glioblastoma-infiltrating myeloid cells using zirconium-89 labeled anti-CD11b antibody. Mol Imaging Biol. 2020; 22: 685-94.
58. Cheng J, Liu W, Zeng X, Zhang B, Guo Y, Qiu M, et al. XRCC3 is a promising target to improve the radiotherapy effect of esophageal squamous cell carcinoma. Cancer Sci. 2015; 106: 1678-86.
59. Moreno-Acosta P, Vallard A, Carrillo S, Gamboa O, Romero-Rojas A, Molano M, et al. Biomarkers of resistance to radiation therapy: a prospective study in cervical carcinoma. Radiat Oncol. 2017; 12: 120.
60. Larionova I, Rakina M, Ivanyuk E, Trushchuk Y, Chernyshova A, Denisov E. Radiotherapy resistance: identifying universal biomarkers for various human cancers. J Cancer Res Clin Oncol. 2022; 148: 1015-31.
61. Zhu L, Zhao Y, Liu T, Chen M, Qian WP, Jiang B, et al. Inhibition of NADPH oxidase-ROS signal using hyaluronic acid nanoparticles for overcoming radioresistance in cancer therapy. ACS Nano. 2022; 16: 18708-28.
62. Martin-Saldaña S, Chevalier MT, Pandit A. Therapeutic potential of targeting galectins - a biomaterials-focused perspective. Biomaterials. 2022; 286: 121585.
63. Jeon H-M, Kim J-Y, Cho HJ, Lee WJ, Nguyen D, Kim SS, et al. Tissue factor is a critical regulator of radiation therapy-induced glioblastoma remodeling. Cancer Cell. 2023; 41: 1480-97.
64. Tolmachev V, Malmberg J, Hofström C, Abrahmsén L, Bergman T, Sjöberg A, et al. Imaging of insulinlike growth factor type 1 receptor in prostate cancer xenografts using the affibody molecule 111In-DOTA-ZIGF1R:4551. J Nucl Med. 2012; 53: 90-7.
65. Steinkamp PJ, Pranger BK, Li MF, Linssen MD, Voskuil FJ, Been LB, et al. Fluorescence-guided visualization of soft-tissue sarcomas by targeting vascular endothelial growth factor A: a phase 1 single-center clinical trial. J Nucl Med. 2021; 62: 342-7.
66. Zhang YQ, Liu WL, Luo XJ, Shi JP, Zeng YZ, Chen WL, et al. Novel self-assembled multifunctional nanoprobes for second-near-infrared-fluorescence-image-guided breast cancer surgery and enhanced radiotherapy efficacy. Adv Sci (Weinh). 2023; 10: 2205294.
67. Wu F, Liu J, Tao M, Wang M, Ren X, Hai Z. β-Galactosidase-activatable fluorescent and photoacoustic imaging of tumor senescence. Anal Chem. 2023; 95: 10481-5.
68. Zhang J, He T, Xue L, Guo H. Senescent T cells: a potential biomarker and target for cancer therapy. EBioMedicine. 2021; 68: 103409.
69. Kim JH, Brown SL, Gordon MN. Radiation-induced senescence: therapeutic opportunities. Radiat Oncol. 2023; 18: 10.
70. Yu Q, Zhang L, Jiang M, Xiao L, Xiang Y, Wang R, et al. An NIR fluorescence turn-on and MRI bimodal probe for concurrent real-time in vivo sensing and labeling of β-galactosidase. Angew Chem Int Ed Engl. 2023; 62: 202313137.
71. Benadjaoud MA, Soysouvanh F, Tarlet G, Paget V, Buard V, Santos de Andrade H, et al. Deciphering the dynamic molecular program of radiation-induced endothelial senescence. Int J Radiat Oncol Biol Phys. 2022; 112: 975-85.
72. Monteiro C, Miarka L, Perea-García M, Priego N, García-Gómez P, Álvaro-Espinosa L, et al. Stratification of radiosensitive brain metastases based on an actionable S100A9/RAGE resistance mechanism. Nat Med. 2022; 28: 752-65.
73. Price JM, Prabhakaran A, West CML. Predicting tumour radiosensitivity to deliver precision radiotherapy. Nat Rev Clin Oncol. 2023; 20: 83-98.
74. Zhang T, Zhang Y, Zhao Y, Song R, Wang Y, Li K, et al. Annotation of CD8(+) T-cell function via ICAM-1 imaging identifies FAK inhibition as an adjuvant to augment the antitumor immunity of radiotherapy. Theranostics. 2024; 14: 699-713.
75. Zhang Y, Deshane JS, Yang ES, Larimer B. A novel translational PET imaging approach to quantifying abscopal immune activation following targeted

radiotherapy and checkpoint blockade. Int J Radiat Oncol Biol Phys. 2024; 118: 1217-27.
76. Nelson BE, Adashek JJ, Sheth AA, Subbiah V. Predicting the abscopal effect: associated tumor histologic subtypes and biomarkers. Mol Cancer Ther. 2023; 22: 706-16.
77. Gibson HM, McKnight BN, Malysa A, Dyson G, Wiesend WN, McCarthy CE, et al. IFNγ PET imaging as a predictive tool for monitoring response to tumor immunotherapy. Cancer Res. 2018; 78: 5706-17.
78. Nelson BE, Adashek JJ, Lin SH, Subbiah V. The abscopal effect in patients with cancer receiving immunotherapy. Med. 2023; 4: 233-44.
79. Zhao Y, Zhang T, Wang Y, Lu D, Du J, Feng X, et al. ICAM-1 orchestrates the abscopal effect of tumor radiotherapy. Proc Natl Acad Sci U S A. 2021; 118: 2010333118.
80. Sheva K, Roy Chowdhury S, Kravchenko-Balasha N, Meirovitz A. Molecular changes in breast cancer induced by radiation therapy. Int J Radiat Oncol Biol Phys, in press, doi: 10.1016/j.ijrobp.2024.03.019.
81. Ngwa W, Irabor OC, Schoenfeld JD, Hesser J, Demaria S, Formenti SC. Using immunotherapy to boost the abscopal effect. Nat Rev Cancer. 2018; 18: 313-22.
82. Nishiga Y, Drainas AP, Baron M, Bhattacharya D, Barkal AA, Ahrari Y, et al. Radiotherapy in combination with CD47 blockade elicits a macrophage-mediated abscopal effect. Nat Cancer. 2022; 3: 1351-66.
83. Hsieh RC, Krishnan S, Wu RC, Boda AR, Liu A, Winkler M, et al. ATR-mediated CD47 and PD-L1 up-regulation restricts radiotherapy-induced immune priming and abscopal responses in colorectal cancer. Sci Immunol. 2022; 7: eabl9330.
84. Ye ZH, Yu WB, Huang MY, Chen J, Lu JJ. Building on the backbone of CD47-based therapy in cancer: combination strategies, mechanisms, and future perspectives. Acta Pharm Sin B. 2023; 13: 1467-87.
85. Chen D, Verma V, Patel RR, Barsoumian HB, Cortez MA, Welsh JW. Absolute lymphocyte count predicts abscopal responses and outcomes in patients receiving combined immunotherapy and radiation therapy: analysis of 3 phase 1/2 trials. Int J Radiat Oncol Biol Phys. 2020; 108: 196-203.
86. Shi C, Zhang Q, Yao Y, Zeng F, Du C, Nijiati S, et al. Targeting the activity of T cells by membrane surface redox regulation for cancer theranostics. Nat Nanotechnol. 2023; 18: 86-97.
87. Koyasu N, Hyodo F, Iwasaki R, Eto H, Elhelaly AE, Tomita H, et al. Spatiotemporal imaging of redox status using in vivo dynamic nuclear polarization magnetic resonance imaging system for early monitoring of response to radiation treatment of tumor. Free Radic Biol Med. 2022; 179: 170-80.
88. Hecht F, Zocchi M, Alimohammadi F, Harris IS. Regulation of antioxidants in cancer. Mol Cell. 2024; 84: 23-33.
89. Qin X, Jiang H, Liu Y, Zhang H, Tian M. Radionuclide imaging of apoptosis for clinical application. Eur J Nucl Med Mol Imaging. 2022; 49: 1345-59.
90. Fang J, Zhao Y, Wang A, Zhang Y, Cui C, Ye S, et al. In vivo quantitative assessment of a radiation dose based on ratiometric photoacoustic imaging of tumor apoptosis. Anal Chem. 2022; 94: 5149-58.
91. Huang Q, Li F, Liu X, Li W, Shi W, Liu FF, et al. Caspase 3-mediated stimulation of tumor cell repopulation during cancer radiotherapy. Nat Med. 2011; 17: 860-6.
92. Braman N, Prasanna P, Bera K, Alilou M, Khorrami M, Leo P, et al. Novel radiomic measurements of tumor-associated vasculature morphology on clinical imaging as a biomarker of treatment response in multiple cancers. Clin Cancer Res. 2022; 28: 4410-24.
93. Alilou M, Khorrami M, Prasanna P, Bera K, Gupta A, Viswanathan VS, et al. A tumor vasculature-based imaging biomarker for predicting response and survival in patients with lung cancer treated with checkpoint inhibitors. Sci Adv. 2022; 8: eabq4609.
94. Bakke KM, Meltzer S, Grøvik E, Negård A, Holmedal SH, Mikalsen LTG, et al. Imaging the tumour microenvironment in rectal cancer: decline in tumour blood flow during radiotherapy predicts good outcome. Phys Imaging Radiat Oncol. 2023; 25: 100417.
95. Tylawsky DE, Kiguchi H, Vaynshteyn J, Gerwin J, Shah J, Islam T, et al. P-selectin-targeted nanocarriers induce active crossing of the blood-brain barrier via caveolin-1-dependent transcytosis. Nat Mater. 2023; 22: 391-9.
96. Shan X, Gong X, Li J, Wen J, Li Y, Zhang Z. Current approaches of nanomedicines in the market and various stage of clinical translation. Acta Pharm Sin B. 2022; 12: 3028-48.
97. Ha B, Liang K, Liu C, Melemenidis S, Manjappa R, Viswanathan V, et al. Real-time optical oximetry during FLASH radiotherapy using a phosphorescent nanoprobe. Radiother Oncol. 2022; 176: 239-43.
98. Shen X, Pan D, Gong Q, Gu Z, Luo K. Enhancing drug penetration in solid tumors via nanomedicine: evaluation models, strategies and perspectives. Bioact Mater. 2024; 32: 445-72.
99. Gu L, Duan Z, Chen X, Li X, Luo Q, Bhamra A, et al. A transformable amphiphilic and block polymer-dendron conjugate for enhanced tumor penetration and retention with cellular homeostasis perturbation via membrane flow. Adv Mater. 2022; 34: 2200048.
100. Jiang L, Qin D, Zhang C, Cui J, Xu X, Hu R, et al. Poly(N-isopropylacrylamide) microgel-based sensor for clinical-level X-ray dose measurements. ACS Appl Polym Mater. 2023; 5: 10073-80.
101. Pushpavanam K, Dutta S, Inamdar S, Bista T, Sokolowski T, Rapchak A, et al. Versatile detection and monitoring of ionizing radiation treatment using radiation-responsive gel nanosensors. ACS Appl Mater Interfaces. 2022; 14: 14997-5007.
102. Pushpavanam K, Dutta S, Zhang N, Ratcliff T, Bista T, Sokolowski T, et al. Radiation-responsive amino acid nanosensor gel (RANG) for radiotherapy monitoring and trauma care. Bioconjug Chem. 2021; 32: 1984-98.
103. Hong Z, Chen Z, Chen Q, Yang H. Advancing X-ray luminescence for imaging, biosensing, and theragnostics. Acc Chem Res. 2023; 56: 37-51.
104. Gan N, Zou X, Dong M, Wang Y, Wang X, Lv A, et al. Organic phosphorescent scintillation from copolymers by X-ray irradiation. Nat Commun. 2022; 13: 3995.
105. Pratt EC, Skubal M, Mc Larney B, Causa-Andrieu P, Das S, Sawan P, et al. Prospective testing of clinical Cerenkov luminescence imaging against standard-of-care nuclear imaging for tumour location. Nat Biomed Eng. 2022; 6: 559-68.
106. Rosenkrans ZT, Hsu JC, Aluicio-Sarduy E, Barnhart TE, Engle JW, Cai W. Amplification of Cerenkov luminescence using semiconducting polymers for cancer theranostics. Adv Funct Mater. 2023; 33: 2302777.
107. Huang J, Su L, Xu C, Ge X, Zhang R, Song J, Pu K. Molecular radio afterglow probes for cancer radiodynamic theranostics. Nat Mater. 2023; 22: 1421-9.
108. Gawne PJ, Man F, Blower PJ, R TMdR. Direct cell radiolabeling for in vivo cell tracking with PET and SPECT imaging. Chem Rev. 2022; 122: 10266-318.
109. Walle T, Kraske JA, Liao B, Lenoir B, Timke C, von Bohlen Und Halbach E, et al. Radiotherapy orchestrates natural killer cell dependent antitumor immune responses through CXCL8. Sci Adv. 2022; 8: eabh4050.
110. Hall WA, Paulson E, Li XA, Erickson B, Schultz C, Tree A, et al. Magnetic resonance linear accelerator technology and adaptive radiation therapy: an overview for clinicians. CA Cancer J Clin. 2022; 72: 34-56.
111. Salem A. Hypoxia-targeted dose painting in radiotherapy. Semin Radiat Oncol. 2023; 33: 298-306.
112. Wass G, Clifford K, Subramaniam RM. Evaluation of the diagnostic accuracy of FAPI PET/CT in oncologic studies: systematic review and metaanalysis. J Nucl Med. 2023; 64: 1218-24.
113. Natarajan A, Khan S, Liang X, Nguyen H, Das N, Anders D, et al. Preclinical evaluation of (89)Zr-panitumumab for biology-guided radiation therapy. Int J Radiat Oncol Biol Phys. 2023; 116: 927-34.
114. Perlow HK, Nalin AP, Handley D, Gokun Y, Blakaj DM, Beyer SJ, et al. A prospective registry study of (68)Ga-DOTATATE PET/CT incorporation into treatment planning of intracranial meningiomas. Int J Radiat Oncol Biol Phys. 2024; 118: 979-85.
115. Lawal IO, Jani AB, Adediran OA, Goyal S, Abiodun-Ojo OA, Dhere VR, et al. Differences in failure-free survival after salvage radiotherapy guided by conventional imaging versus (18)F-fluciclovine PET/CT in postprostatectomy patients: a post hoc substratification analysis of the EMPIRE-1 Trial. J Nucl Med. 2023; 64: 586-91.
116. Grosu AL, Weber WA, Franz M, Stärk S, Piert M, Thamm R, et al. Reirradiation of recurrent high-grade gliomas using amino acid PET (SPECT)/CT/MRI image fusion to determine gross tumor volume for stereotactic fractionated radiotherapy. Int J Radiat Oncol Biol Phys. 2005; 63: 511-9.
117. Laprie A, Noel G, Chaltiel L, Truc G, Sunyach MP, Charissoux M, et al. Randomized phase III trial of metabolic imaging-guided dose escalation of radio-chemotherapy in patients with newly diagnosed glioblastoma (SPECTRO GLIO trial). Neuro Oncol. 2024; 26: 153-63.
118. van Houdt PJ, Li S, Yang Y, van der Heide UA. Quantitative MRI on MR-Linacs: towards biological image-guided adaptive radiotherapy. Semin Radiat Oncol. 2024; 34: 107-19.
119. Dmochowska N, Milanova V, Mukkamala R, Chow KK, Pham NTH, Srinivasarao M, et al. Nanoparticles targeted to fibroblast activation protein outperform PSMA for MRI delineation of primary prostate tumors. Small. 2023; 19: 2204956.
120. Yuan M, Fang X, Wu Y, Xu Y, Feng H, Mu J, et al. Activatable nanoprobe with aggregation-induced dual fluorescence and photoacoustic signal enhancement for tumor precision imaging and radiotherapy. Anal Chem. 2022; 94: 5204-11.
121. Zhou H, Guo M, Li J, Qin F, Wang Y, Liu T, et al. Hypoxia-triggered self-assembly of ultrasmall iron oxide nanoparticles to amplify the imaging signal of a tumor. J Am Chem Soc. 2021; 143: 1846-53.
122. Geng H, Chen K, Cao L, Liu L, Huang Y, Liu J. Hypoxia-responsive aggregation of gold nanoparticles for near-infrared-II photoacoustic imaging-guided enhanced radiotherapy. Langmuir. 2023; 39: 4037-48.
123. El Naqa I, Pogue BW, Zhang R, Oraiqat I, Parodi K. Image guidance for FLASH radiotherapy. Med Phys. 2022; 49: 4109-22.
124. Tran VL, Lux F, Tournier N, Jego B, Maître X, Anisorac M, et al. Quantitative tissue pharmacokinetics and EPR effect of AGUIX nanoparticles: a multimodal imaging study in an orthotopic glioblastoma rat model and healthy macaque. Adv Healthc Mater. 2021; 10: 2100656.
125. Chiarelli PA, Revia RA, Stephen ZR, Wang K, Kievit FM, Sandhu J, et al. Iron oxide nanoparticle-mediated radiation delivery for glioblastoma treatment. Mater Today. 2022; 56: 66-78.
126. Lavielle A, Boux F, Deborne J, Pinaud N, Dufort S, Verry C, et al. T(1) mapping from MPRAGE acquisitions: application to the measurement of the concentration of nanoparticles in tumors for theranostic use. J Magn Reson Imaging. 2023; 58: 313-23.
127. Keall PJ, Brighi C, Glide-Hurst C, Liney G, Liu PZY, Lydiard S, et al. Integrated MRI-guided radiotherapy — opportunities and challenges. Nat Rev Clin Oncol. 2022; 19: 458-70.
128. Akcay K, Kibar A, Sahin OE, Demirbilek M, Beydagi G, Asa S, et al. Prediction of clinically significant prostate cancer by [(68) Ga]Ga-PSMA-11 PET/CT: a

potential tool for selecting patients for active surveillance. Eur J Nucl Med Mol Imaging. 2024; 51: 1467-75.
129. Park S, Parihar AS, Bodei L, Hope TA, Mallak N, Millo C, et al. Somatostatin receptor imaging and theranostics: current practice and future prospects. J Nucl Med. 2021; 62: 1323-9.
130. Hope TA, Antonarakis ES, Bodei L, Calais J, Iravani A, Jacene H, et al. SNMMI consensus statement on patient selection and appropriate use of (177)Lu-PSMA-617 radionuclide therapy. J Nucl Med. 2023; 64: 1417-23.
131. Spohn SKB, Schmidt-Hegemann NS, Ruf J, Mix M, Benndorf M, Bamberg F, et al. Development of PSMA-PET-guided CT-based radiomic signature to predict biochemical recurrence after salvage radiotherapy. Eur J Nucl Med Mol Imaging. 2023; 50: 2537-47.
132. Jo J, Folz J, Gonzalez ME, Paolì A, Eido A, Salfi E, et al. Personalized oncology by in vivo chemical imaging: photoacoustic mapping of tumor oxygen predicts radiotherapy efficacy. ACS Nano. 2023; 17: 4396-403.
133. Wu L, Ishigaki Y, Zeng W, Harimoto T, Yin B, Chen Y, et al. Generation of hydroxyl radical-activatable ratiometric near-infrared bimodal probes for early monitoring of tumor response to therapy. Nat Commun. 2021; 12: 6145.
134. Fu Q, Feng H, Su L, Zhang X, Liu L, Fu F, et al. An activatable hybrid organic-inorganic nanocomposite as early evaluation system of therapy effect. Angew Chem Int Ed Engl. 2022; 61: 202112237.
135. Rich LJ, Miller A, Singh AK, Seshadri M. Photoacoustic imaging as an early biomarker of radio therapeutic efficacy in head and neck cancer. Theranostics. 2018; 8: 2064-78.
136. Ge X, Su L, Chen Z, Zhu K, Zhang X, Wu Y, Song J. A radio-pharmaceutical fluorescent probe for synergistic cancer radiotherapy and ratiometric imaging of tumor reactive oxygen species. Angew Chem Int Ed Engl. 2023; 62: 202305744.
137. Goryawala M, Mellon EA, Shim H, Maudsley AA. Mapping early tumor response to radiotherapy using diffusion kurtosis imaging*. Neuroradiol J. 2023; 36: 198-205.
138. Wang C, Padgett KR, Su MY, Mellon EA, Maziero D, Chang Z. Multi-parametric MRI (mpMRI) for treatment response assessment of radiation therapy. Med Phys. 2022; 49: 2794-819.
139. Hu K, Wu W, Xie L, Geng H, Zhang Y, Hanyu M, et al. Whole-body PET tracking of a d-dodecapeptide and its radiotheranostic potential for PD-L1 overexpressing tumors. Acta Pharm Sin B. 2022; 12: 1363-76.
140. van der Veen EL, Suurs FV, Cleeren F, Bormans G, Elsinga PH, Hospers GAP, et al. Development and evaluation of interleukin-2-derived radiotracers for PET imaging of T cells in mice. J Nucl Med. 2020; 61: 1355-60.
141. Oyoshi H, Du J, Sakai SA, Yamashita R, Okumura M, Motegi A, et al. Comprehensive single-cell analysis demonstrates radiotherapy-induced infiltration of macrophages expressing immunosuppressive genes into tumor in esophageal squamous cell carcinoma. Sci Adv. 2023; 9: eadh9069.
142. Cheng X, Shen J, Xu J, Zhu J, Xu P, Wang Y, Gao M. In vivo clinical molecular imaging of T cell activity. Trends Immunol. 2023; 44: 1031-45.
143. Song X, Zhang Y, Lv X, Xu Z, Long Y, Gai Y, et al. Noninvasive longitudinal PET/CT imaging of CAR T cells using PSMA reporter gene. Eur J Nucl Med Mol Imaging. 2024; 51: 965-77.
144. Laurent PA, Morel D, Meziani L, Depil S, Deutsch E. Radiotherapy as a means to increase the efficacy of T-cell therapy in solid tumors. Oncoimmunology. 2023; 12: 2158013.
145. Croci D, Santalla Méndez R, Temme S, Soukup K, Fournier N, Zomer A, et al. Multispectral fluorine-19 MRI enables longitudinal and noninvasive monitoring of tumor-associated macrophages. Sci Transl Med. 2022; 14: eabo2952.
146. Luo X, Hu D, Gao D, Wang Y, Chen X, Liu X, et al. Metabolizable near-infrared-II nanoprobes for dynamic imaging of deep-seated tumor-associated macrophages in pancreatic cancer. ACS Nano. 2021; 15: 10010-24.
147. Liu X, Wang M, Jiang Y, Zhang X, Shi C, Zeng F, et al. Magnetic resonance imaging nanoprobe quantifies nitric oxide for evaluating M1/M2 macrophage polarization and prognosis of cancer treatments. ACS Nano. 2023; 17: 24854-66.
148. Kuang J, Rao ZY, Zheng DW, Kuang D, Huang QX, Pan T, et al. Nanoparticles hitchhike on monocytes for glioblastoma treatment after low-dose radiotherapy. ACS Nano. 2023; 17: 13333-47.
149. He S, Cheng P, Pu K. Activatable near-infrared probes for the detection of specific populations of tumour-infiltrating leukocytes in vivo and in urine. Nat Biomed Eng. 2023; 7: 281-97.
150. Zheng X, Cui L, Chen M, Soto LA, Graves EE, Rao J. A near-infrared phosphorescent nanoprobe enables quantitative, longitudinal imaging of tumor hypoxia dynamics during radiotherapy. Cancer Res. 2019; 79: 4787-97.
151. Cao X, Allu SR, Jiang S, Gunn Bs JR, Yao Ph DC, Xin Ph DJ, et al. High-resolution pO(2) imaging improves quantification of the hypoxic fraction in tumors during radiation therapy. Int J Radiat Oncol Biol Phys. 2021; 109: 603-13.
152. An Y, Gu W, Miao M, Miao J, Zhou H, Zhao M, et al. A self-assembled organic probe with activatable near-infrared fluoro-photoacoustic signals for in vivo evaluation of the radiotherapy effect. Anal Chem. 2023; 95: 13984-91.
153. Xu H, Wang Y, Zhang J, Duan X, Zhang T, Cai X, et al. A self-triggered radioligand therapy agent for fluorescence imaging of the treatment response in prostate cancer. Eur J Nucl Med Mol Imaging. 2022; 49: 2693-704.
154. Dou Y, Zhao F, Li X, Guo Y. Monitoring nitric oxide-induced hypoxic tumor radiosensitization by radiation-activated nanoagents under BOLD/DWI imaging. ACS Biomater Sci Eng. 2021; 7: 5242-54.
155. Johnson BJ, Barcus RA, Olson JD, Lipford ME, Andrews RN, Dugan GO, et al. Total-body irradiation alters white matter volume and microstructural integrity in rhesus macaques. Int J Radiat Oncol Biol Phys. 2024; 119: 208-18.
156. Saednia K, Tabbarah S, Lagree A, Wu T, Klein J, Garcia E, et al. Quantitative thermal imaging biomarkers to detect acute skin toxicity from breast radiation therapy using supervised machine learning. Int J Radiat Oncol Biol Phys. 2020; 106: 1071-83.
157. Barazzuol L, Coppes RP, van Luijk P. Prevention and treatment of radiotherapy-induced side effects. Mol Oncol. 2020; 14: 1538-54.
158. Chamseddine I, Kim Y, De B, El Naqa I, Duda DG, Wolfgang J, et al. Predictive modeling of survival and toxicity in patients with hepatocellular carcinoma after radiotherapy. JCO Clin Cancer Inform. 2022; 6: 2100169.
159. Alam SR, Zhang P, Zhang SY, Chen I, Rimner A, Tyagi N, et al. Early prediction of acute esophagitis for adaptive radiation therapy. Int J Radiat Oncol Biol Phys. 2021; 110: 883-92.
160. Evanson D, Griffin M, O'Reilly SE, Johnson T, Werner T, Kothekar E, et al. Comparative assessment of radiation therapy-induced vasculitis using [(18)F]FDG-PET/CT in patients with non-small cell lung cancer treated with proton versus photon radiotherapy. Eur J Nucl Med Mol Imaging. 2024; 51: 1444-50.
161. Park H, Tseng SC, Sholl LM, Hatabu H, Awad MM, Nishino M. Molecular characterization and therapeutic approaches to small cell lung cancer: imaging implications. Radiology. 2022; 305: 512-25.
162. Chen T, Zhuang B, Huang Y, Liu Y, Yuan B, Wang W, et al. Inhaled curcumin mesoporous polydopamine nanoparticles against radiation pneumonitis. Acta Pharm Sin B. 2022; 12: 2522-32.
163. Pei J, Cheng K, Liu T, Gao M, Wang S, Xu S, et al. Early, non-invasive detection of radiation-induced lung injury using PET/CT by targeting CXCR4. Eur J Nucl Med Mol Imaging. 2024; 51: 1109-20.
164. Saleem A, Helo Y, Win Z, Dale R, Cook J, Searle GE, Wells P. Integrin αvβ6 positron emission tomography imaging in lung cancer patients treated with pulmonary radiation therapy. Int J Radiat Oncol Biol Phys. 2020; 107: 370-6.
165. Abston E, Zhou IY, Saenger JA, Shuvaev S, Akam E, Esfahani SA, et al. Noninvasive quantification of radiation-induced lung injury using a targeted molecular imaging probe. Int J Radiat Oncol Biol Phys. 2024; 118: 1228-39.
166. Plana JC, Galderisi M, Barac A, Ewer MS, Ky B, Scherrer-Crosbie M, et al. Expert consensus for multimodality imaging evaluation of adult patients during and after cancer therapy: a report from the American Society of Echocardiography and the European Association of Cardiovascular Imaging. J Am Soc Echocardiogr. 2014; 27: 911-39.
167. No HJ, Guo FB, Park NJ, Kastelowitz N, Rhee JW, Clark DE, et al. Predicting adverse cardiac events after radiotherapy for locally advanced non-small cell lung cancer. JACC CardioOncol. 2023; 5: 775-87.
168. Chalubinska-Fendler J, Graczyk L, Piotrowski G, Wyka K, Nowicka Z, Tomasik B, et al. Lipopolysaccharide-binding protein is an early biomarker of cardiac function after radiation therapy for breast cancer. Int J Radiat Oncol Biol Phys. 2019; 104: 1074-83.
169. Totzeck M, Aide N, Bauersachs J, Bucerius J, Georgoulias P, Herrmann K, et al. Nuclear medicine in the assessment and prevention of cancer therapy-related cardiotoxicity: prospects and proposal of use by the European Association of Nuclear Medicine (EANM). Eur J Nucl Med Mol Imaging. 2023; 50: 792-812.
170. Kersting D, Mavroeidi IA, Settelmeier S, Seifert R, Schuler M, Herrmann K, et al. Molecular imaging biomarkers in cardiooncology: a view on established technologies and future perspectives. J Nucl Med. 2023; 64: 29s-38s.
171. Diekmann J, Koenig T, Thackeray JT, Derlin T, Czerner C, Neuser J, et al. Cardiac fibroblast activation in patients early after acute myocardial infarction: integration with MR tissue characterization and subsequent functional outcome. J Nucl Med. 2022; 63: 1415-23.
172. Siebermair J, Köhler MI, Kupusovic J, Nekolla SG, Kessler L, Ferdinandus J, et al. Cardiac fibroblast activation detected by Ga-68 FAPI PET imaging as a potential novel biomarker of cardiac injury/remodeling. J Nucl Cardiol. 2021; 28: 812-21.
173. Wei Y, Sun Y, Liu J, Zhang G, Qin X, Xu S, et al. Early detection of radiation-induced myocardial damage by [(18)F]AlF-NOTA-FAPI-04 PET/CT imaging. Eur J Nucl Med Mol Imaging. 2023; 50: 453-64.
174. Cousins MM, Devasia TP, Maurino CM, Mikell J, Schipper MJ, Kaza RK, et al. Pretreatment levels of soluble tumor necrosis factor receptor 1 and hepatocyte growth factor predict toxicity and overall survival after (90)Y radioembolization: potential novel application of biomarkers for personalized management of hepatotoxicity. J Nucl Med. 2022; 63: 882-9.
175. Li M, Robles-Planells C, Liu D, Graves SA, Vasquez-Martinez G, Mayoral-Andrade G, et al. Pre-clinical evaluation of biomarkers for the early detection of nephrotoxicity following alpha-particle radioligand therapy. Eur J Nucl Med Mol Imaging. 2024; 51: 1395-408.
176. Lu D, Zhou H, Li N, Wang Y, Zhang T, Wang F, et al. Galectin expression detected by (68)Ga-galectracer PET as a predictive biomarker of radiotherapy resistance. Eur J Nucl Med Mol Imaging. 2022; 49: 2746-60.
177. Hu K, Li J, Wang L, Huang Y, Li L, Ye S, et al. Preclinical evaluation and pilot clinical study of [(18)F]AlF-labeled FAPI-tracer for PET imaging of cancer associated fibroblasts. Acta Pharm Sin B. 2022; 12: 867-75.

178. Li M, Younis MH, Zhang Y, Cai W, Lan X. Clinical summary of fibroblast activation protein inhibitor-based radiopharmaceuticals: cancer and beyond. Eur J Nucl Med Mol Imaging. 2022; 49: 2844-68.
179. Gonzalez-Junca A, Reiners O, Borrero-Garcia LD, Beckford-Vera D, Lazar AA, Chou W, et al. Positron emission tomography imaging of functional transforming growth factor β (TGFβ) activity and benefit of TGFβ inhibition in irradiated intracranial tumors. Int J Radiat Oncol Biol Phys. 2021; 109: 527-39.
180. Ludwig JA, Weinstein JN. Biomarkers in cancer staging, prognosis and treatment selection. Nat Rev Cancer. 2005; 5: 845-56.
181. Ortmann J, Rampášek L, Tai E, Mer AS, Shi R, Stewart EL, et al. Assessing therapy response in patient-derived xenografts. Sci Transl Med. 2021; 13: eabf4969.
182. Dreyfuss AD, Goia D, Shoniyozov K, Shewale SV, Velalopoulou A, Mazzoni S, et al. A novel mouse model of radiation-induced cardiac injury reveals biological and radiological biomarkers of cardiac dysfunction with potential clinical relevance. Clin Cancer Res. 2021; 27: 2266-76.
183. Landgraf M, McGovern JA, Friedl P, Hutmacher DW. Rational design of mouse models for cancer research. Trends Biotechnol. 2018; 36: 242-51.
184. Bera K, Braman N, Gupta A, Velcheti V, Madabhushi A. Predicting cancer outcomes with radiomics and artificial intelligence in radiology. Nat Rev Clin Oncol. 2022; 19: 132-46.
185. Schoenfeld JD, Giobbie-Hurder A, Ranasinghe S, Kao KZ, Lako A, Tsuji J, et al. Durvalumab plus tremelimumab alone or in combination with low-dose or hypofractionated radiotherapy in metastatic non-small-cell lung cancer refractory to previous PD(L)-1 therapy: an open-label, multicentre, randomised, phase 2 trial. Lancet Oncol. 2022; 23: 279-91.
186. Strosberg J, Hofman MS, Al-Toubah T, Hope TA. Rethinking dosimetry: the perils of extrapolated external-beam radiotherapy constraints to radionuclide therapy. J Nucl Med. 2024; 65: 362-4.
187. Frascogna C, Mottareale R, La Verde G, Arrichiello C, Muto P, Netti PA, et al. Role of the mechanical microenvironment on CD-44 expression of breast adenocarcinoma in response to radiotherapy. Sci Rep. 2024; 14: 391.
188. Suzuki H, Araki M, Tatsugi K, Ichinohe K, Uehara T, Arano Y. Reduction of the renal radioactivity of (111)In-DOTA-labeled antibody fragments with a linkage cleaved by the renal brush border membrane enzymes. J Med Chem. 2023; 66: 8600-13.
189. Xiang Y, Wang B, Yang W, Zheng X, Chen R, Gong Q, et al. Mitocytosis mediated by an enzyme-activable mitochondrion-disturbing polymer-drug conjugate enhances active penetration in glioblastoma therapy. Adv Mater. 2024; 36: 2311500.
190. Zhang P, Xu M, Ding J, Chen J, Zhang T, Huo L, Liu Z. Fatty acid-conjugated radiopharmaceuticals for fibroblast activation protein-targeted radiotherapy. Eur J Nucl Med Mol Imaging. 2022; 49: 1985-96.
191. Li H, Feng Y, Luo Q, Li Z, Li X, Gan H, et al. Stimuli-activatable nanomedicine meets cancer theranostics. Theranostics. 2023; 13: 5386-417.
192. Lammers T. Nanomedicine tumor targeting. Adv Mater. 2024; 36: 2312169.
193. Xu M, Qi Y, Liu G, Song Y, Jiang X, Du B. Size-dependent in vivo transport of nanoparticles: implications for delivery, targeting, and clearance. ACS Nano. 2023; 17: 20825-49.
194. Sritharan K, Akhiat H, Cahill D, Choi S, Choudhury A, Chung P, et al. Development of prostate bed delineation consensus guidelines for magnetic resonance image-guided radiotherapy and assessment of its effect on interobserver variability. Int J Radiat Oncol Biol Phys. 2024; 118: 378-89.
195. Ahunbay EE, Thapa R, Chen X, Paulson E, Li XA. A technique to rapidly generate synthetic computed tomography for magnetic resonance imaging-guided online adaptive replanning: an exploratory study. Int J Radiat Oncol Biol Phys. 2019; 103: 1261-70.
196. Tran-Gia J, Salas-Ramirez M, Lassmann M. What you see is not what you get: on the accuracy of voxel-based dosimetry in molecular radiotherapy. J Nucl Med. 2020; 61: 1178-86.
197. Tan P, Chen X, Zhang H, Wei Q, Luo K. Artificial intelligence aids in development of nanomedicines for cancer management. Semin Cancer Biol. 2023; 89: 61-75.
198. Zhang Y, Hu HH, Zhou SH, Xia WY, Zhang Y, Zhang JP, et al. PET-based radiomics visualizes tumor-infiltrating CD8 T cell exhaustion to optimize radiotherapy/immunotherapy combination in mouse models of lung cancer. Biomark Res. 2023; 11: 10.
199. Miao L, Cao Y, Zuo L, Zhang H, Guo C, Yang Z, et al. Predicting pathological complete response of neoadjuvant radiotherapy and targeted therapy for soft tissue sarcoma by whole-tumor texture analysis of multisequence MRI imaging. Eur Radiol. 2023; 33: 3984-94.